Openventio PUBLISHERS

ISSN 2473-0947

RADIOLOGY

Open Journal

| May 2016 | Volume 1 | Issue 1 |

www.openventio.org

RADIOLOGY

Openventio PUBLISHERS

ISSN 2473-0947

Open Journal

TABLE OF CONTENTS

RADIOLOGY

Openventio PUBLISHERS

ISSN 2473-0947 Open Journal http://dx.doi.org/10.17140/ROJ-1-e001

Editorial

*Corresponding author
Alessandro Arrigo, MD
Department of Biomedical Sciences and Morphological and Functional Imaging
University of Messina
Via Consolare Valeria
1 Messina, 98125, Italy
Tel. +39 0902212939
E-mail: alessandro.arrigo@hotmail.com

Volume 1 : Issue 1
Article Ref. #: 1000ROJ1e001

Article History
Received: November 5th, 2015
Accepted: November 6th, 2015
Published: November 9th, 2015

Citation
Arrigo A, Mormina E, Calamuneri A. The pre-surgical planning of brain neoplasms: from diffusion tensor imaging to more advanced approaches. *Radiol Open J*. 2015; 1(1): e1-e5. doi: 10.17140/ROJ-1-e001

The Pre-Surgical Planning of Brain Neoplasms: From Diffusion Tensor Imaging to More Advanced Approaches

Alessandro Arrigo*, Enricomaria Mormina and Alessandro Calamuneri

Department of Biomedical Sciences and Morphological and Functional Images, University of Messina, Messina, Italy

KEYWORDS: Brain neoplasm; Tractography; Pre-surgical planning; DTI; CSD.

The pre-surgical planning of brain neoplasms is strongly contributing to change the prognosis of neoplastic patients. Indeed, it supplies more and more detailed and reliable functional and morphological information before as well as during surgery. Both invasive and non-invasive approaches are available to achieve this goal. A powerful technique for the pre-surgical planning of brain neoplasms is Diffusion Weighted Imaging (DWI) based tractography. Differently from other approaches, tractography is able to provide, non-invasively, morphological information regarding brain pathways relationship with the neoplasm, by analyzing water diffusion within white matter. This is important especially for eloquent bundles, such as Cortico-Spinal Tract (CST) and Arcuate Fasciculus (AF), whose damages have a bad impact on the patient's Quality of Life (QoL). Tractography can be performed through several diffusion signal modeling techniques, among which Diffusion Tensor Imaging (DTI) is the most known. DTI has been widely used for neurosurgery both in pre-operative and intra-operative contexts, also in combination with other functional approaches such as functional MRI (fMRI) and cortical stimulation.[1-8] This useful technique was able to reduce post-surgical deficits as well as to improve the survival of neoplastic patients, through a better delineation of maximal safe resection.[9] Moreover, its use provided great benefits in patients with high-grade gliomas in terms of risk of death.[9] Several studies have demonstrated that DTI suffers from many limitations regarding its reliability to correctly model diffusion signal in different conditions.[10,11] Furthermore, tensorial models are not able to resolve different fibers geometries (i.e. crossing fibers) within the same voxel; these complex configurations have been demonstrated to characterize more than 90% of white matter voxels,[12] thus making DTI an unreliable diffusion modeling technique. In order to overcome these limitations, several other approaches were developed; in particular, High Angular Resolution Diffusion-weighted Imaging (HARDI),[13] Q-Ball Imaging (QBI)[14] and Diffusion Spectrum Imaging (DSI)[15] were found to be promising techniques for resolving voxels with multiple fibers orientations. Nevertheless, tractography was further improved by an HARDI modified approach called Constrained Spherical Deconvolution (CSD); this technique does not require very long acquisition time with respect to DSI[16] and it is able to improve angular resolution if compared to QBI.[17] CSD-based tractography was widely used in physiological contexts as well as in pathological ones, showing high sensitivity for the detection of white matter pathways.[18-22] Although tensorial approaches were proved to be inadequate for reliably reconstructing brain pathways[23] and histological validation of CSD-based tractography has been recently provided,[24] more advanced diffusion techniques are still considered not usable in clinical settings due to their too high technical requirements.[25] For these reasons, DTI remains, to date, the most used technique for investigating white matter bundles, also for the pre-surgical planning of brain neoplasms.[26-28] In reality, as recently highlighted by Mormina and colleagues,[29] CSD-based tractography is feasible in clinical settings and it is able to provide very useful information during the pre-surgical evaluation of eloquent bundles in patients with high-grade gliomas. It was shown that DTI-based reconstructions can be affected also by neoplasm's effects on white matter bundles. Indeed, brain pathways might result dislocated, disrupted and/or infiltrated by neoplasm,[30] with simultaneous Fractional Anisotropy (FA) dec-

ISSN 2473-0947 Open Journal http://dx.doi.org/10.17140/ROJ-1-e001

rements; tensorial models are not able to distinguish among these different conditions, thus causing partial reconstructions or null detection of bundles involved. Moreover, peritumoral edema surrounding high-grade gliomas is able to reduce FA values,[31] causing, also in this case, misleading fiber tracking. Mormina, et al.[29] showed how CSD-based tractography is able to clearly define fiber bundles involved by high-grade gliomas. Comparative qualitative analysis between CSD-based tractography and DTI-based one in patients with high-grade gliomas is shown in Figures 1 and 2.

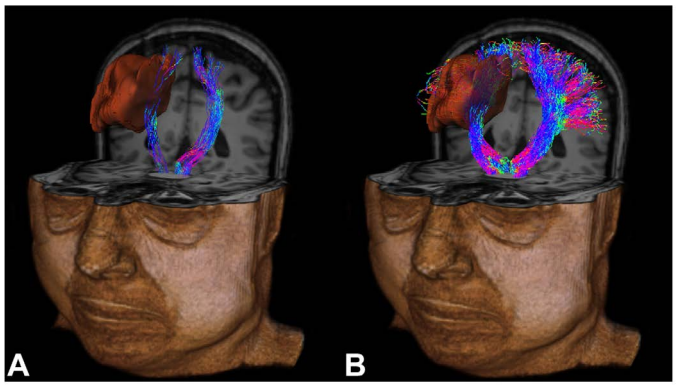

Figure 1: Comparative qualitative analysis of bilateral CST reconstructions in a patient with right high-grade glioma (brown volume). DTI-based tractography (A) shows a good detection of the medial CST portion in the healthy side, whereas it is less represented in the affected side. Lateral CST portions are bilaterally missing. CSD-based tractography (B) shows robust detection of the entire CST in the healthy side. The medial CST portion results poorly involved in the affected side; moreover, the lateral CST portion is still detected, although it seems to be more involved by neoplasm. While the lack of DTI detection of lateral CST might be due to DTI intrinsic limitations, different representations of medial CST in the affected side might be caused by peritumoral edema affecting DTI-based reconstruction.

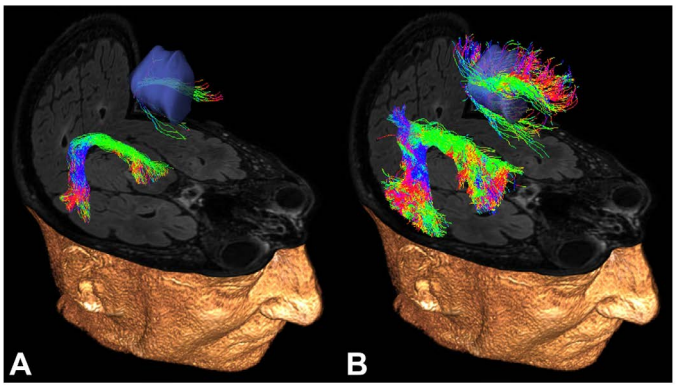

Figure 2: Comparative qualitative analysis of bilateral AF reconstructions in a patient with left high-grade glioma (blue volume). DTI-based tractography (A) shows a good AF detection in the healthy side, although several portions are poorly represented, such as the anterior one. AF seems to be widely damaged by neoplasmin the affected side. CSD-based tractography (B) shows a better detection of all AF portions in the healthy side, if compared to DTI-based one. Moreover, it shows a good AF representation in the affected side; this suggests that AF is involved by neoplasm although it is not strongly damaged. Also in this case, both DTI limitations and peritumoral edema might cause differences regarding AF representations in the affected side, if compared to CSD-based one.

Mormina and colleagues[29] showed also how this technique allowed are liable analysis of diffusion-based parameters of reconstructed pathways in neoplastic patients. The quantitative evaluation of white matter streamlines based on diffusion tensor parameters, such as FA and Mean Diffusivity (MD), is considered another important measurement for detecting structural alterations of white matter caused by a loss of axonal integrity. Since DTI-based tractography does not consider voxels with low FA values, the quantitative analysis might provide the erroneous information of not significant white matter alterations; the latter, together with a partial qualitative analysis of affected pathways, might thus suggest false safe resection margins around the neoplasm. Moreover, it is worthy to note that a pre-surgical planning performed by means of DTI-based tractography cannot provide any qualitative and quantitative information regarding well-known undetected white matter bundles, such as the lateral portion of CST as well as the anterior portion of AF.[29,32] All these limitations might be avoided by using CSD-based approach. Its sensitivity for reconstructing white matter bundles has been also recently highlighted by a comparative analysis of different tractographic approaches; in detail, CSD-based tractography was able to better detect brain pathways involved by neoplasm if compared to DTI-based one.[33]

ISSN 2473-0947 Open Journal http://dx.doi.org/10.17140/ROJ-1-e001

This brief description showed how the use of more advanced DWI-based approaches can provide useful information before surgical treatment of patients with brain neoplasms. It was demonstrated that these techniques are able to improve effectiveness of surgical treatments as well as their outcome by allowing a better delineation of resection margins. Moreover, they may have a good impact on the quality of life of neoplastic patients by helping to preserve eloquent fiber bundles and consequently by reducing post-surgical deficits. Several authors demonstrated that advanced diffusion signal modeling algorithms, such as CSD one, can be compatible with clinical settings and they should be more largely used for pre-surgical planning of brain neoplasms.

Interesting future perspectives for brain neoplasms treatment will regard the combined use of CSD-based tractography with functional approaches, such as neuronavigated Transcranial Magnetic Stimulation (nTMS), in order to further improve detection of eloquent bundles. Indeed, a recent study has adopted nTMS for subject-specific localization of the motor area and then DTI-based tractography for CST tracking; this approach allowed a good detection of CST, although tractographic reconstructions were found affected by above described DTI limitations, such as the peritumoral edema.[34] The use of CSD-based tractography in a similar study protocol might provide a better subject-specific detection of CST. Finally it will be important to assess potential improvements and advantages for neurosurgeons provided by the integration of these techniques into intraoperative navigation systems.

CONFLICTS OF INTEREST

The authors have no conflicts of interest to declare.

CONSENT

Patients has provided written consent for submission of this manuscript for publication.

REFERENCES

1. Berman JI, Berger MS, Mukherjee P, Henry RG. Diffusion-tensor imaging-guided tracking of fibers of the pyramidal tract combined with intraoperative cortical stimulation mapping in patients with gliomas. *J Neurosurg*. 2004; 101(1): 66-72.

2. Coenen VA, Krings T, Mayfrank L, et al. Three-dimensional visualization of the pyramidal tract in a neuronavigation system during brain tumor surgery: first experiences and technical note. *Neurosurgery*. 2001; 49(1): 86-92.

3. Henry RG, Berman JI, Nagarajan SS, Mukherjee P, Berger MS. Subcortical pathways serving cortical language sites: initial experience with diffusion tensor imaging fiber tracking combined with intraoperative language mapping. *Neuroimage*. 2004; 21(2): 616-622. doi: 10.1016/j.neuroimage.2003.09.047

4. Kamada K, Todo T, Masutani Y, et al. Combined use of tractography-integrated functional neuronavigation and direct fiber stimulation. *J Neurosurg*. 2005; 102(4): 664-672.

5. Nimsky C, Ganslandt O, Hastreiter P, et al. Preoperative and intraoperative diffusion tensor imaging-based fiber tracking in glioma surgery. *Neurosurgery*. 2005; 56(1): 130-137; discussion 138.

6. Nimsky C, Ganslandt O, Merhof D, Sorensen AG, Fahlbusch R. Intraoperative visualization of the pyramidal tract by diffusion-tensor-imaging-based fiber tracking. *Neuroimage*. 2006; 30(4): 1219-1229. doi: 10.1016/j.neuroimage.2005.11.001

7. Bello L, Castellano A, Fava E, et al. Intraoperative use of diffusion tensor imaging fiber tractography and subcortical mapping for resection of gliomas: technical considerations. *Neurosurg Focus*. 2010; 28(2): E6. doi: 10.3171/2009.12.FOCUS09240

8. González-Darder JM, González-López P, Talamantes F, et al. Multimodal navigation in the functional microsurgical resection of intrinsic brain tumors located in eloquent motor areas: role of tractography. *Neurosurg Focus*. 2010; 28(2): E5. doi: 10.3171/2009.11.FOCUS09234

9. Wu JS, Zhou LF, Tang WJ, et al. Clinical evaluation and follow-up outcome of diffusion tensor imaging-based functional neuronavigation: a prospective, controlled study in patients with gliomas involving pyramidal tracts. *Neurosurgery*. 2007; 61(5): 935-948.

10. Jones DK, Cercignani M. Twenty-five pitfalls in the analysis of diffusion MRI data. *NMR Biomed*. 2010; 23(7): 803-820. doi: 10.1002/nbm.1543

11. Farquharson S, Tournier JD, Calamante F, et al. White matter fiber tractography: why we need to move beyond DTI. *J Neurosurg*. 2013; 118(6): 1367-1377. doi: 10.3171/2013.2.JNS121294

12. Jeurissen B, Leemans A, Tournier JD, Jones DK, Sijbers J. Investigating the prevalence of complex fiber configurations in white matter tissue with diffusion magnetic resonance imaging. *Hum Brain Mapp*. 2013; 34(11): 2747-2766. doi: 10.1002/hbm.22099

13. Tuch DS, Reese TG, Wiegell MR, Makris N, Belliveau JW, Wedeen VJ. High angular resolution diffusion imaging reveals intravoxel white matter fiber heterogeneity. *Magn Reson Med*. 2002; 48(4): 577-582. doi: 10.1002/mrm.10268

14. Tuch DS. Q-ball imaging. *Magn Reson Med*. 2004; 52(6): 1358-1372. doi: 10.1002/mrm.20279

15. Wedeen VJ, Wang RP, Schmahmann JD, et al. Diffusion spectrum magnetic resonance imaging (DSI) tractography of crossing fibers. *Neuroimage*. 2008; 41(4): 1267-1277. doi: 10.1016/j.neuroimage.2008.03.036

16. Tournier JD, Calamante F, Connelly A. Robust determination of the fibre orientation distribution in diffusion MRI: non-negativity constrained super-resolved spherical deconvolution. *Neuroimage*. 2007; 35(4): 1459-1472. doi: 10.1016/j.neuroimage.2007.02.016

17. Tournier JD, Yeh CH, Calamante F, Cho KH, Connelly A, Lin CP. Resolving crossing fibres using constrained spherical deconvolution: validation using diffusion-weighted imaging phantom data. *Neuroimage*. 2008; 42(2): 617-625. doi: 10.1016/j.neuroimage.2008.05.002

18. Arrigo A, Mormina E, Anastasi GP, et al. Constrained spherical deconvolution analysis of the limbic network in human, with emphasis on a direct cerebello-limbic pathway. *Front Hum Neurosci*. 2014; 8: 987. doi: 10.3389/fnhum.2014.00987

19. Mormina E, Arrigo A, Calamuneri A, et al. Diffusion tensor imaging parameters' changes of cerebellar hemispheres in Parkinson's disease. *Neuroradiology*. 2015; 57(3): 327-334. doi: 10.1007/s00234-014-1473-5

20. Mormina E, Briguglio M, Morabito R, et al. A rare case of cerebellar agenesis: a probabilistic constrained spherical deconvolution tractographic study. *Brain Imaging Behav*. 2015. doi: 10.1007/s11682-015-9377-5

21. Auriat AM, Borich MR, Snow NJ, Wadden KP, Boyd LA. Comparing a diffusion tensor and non-tensor approach to white matter fiber tractography in chronic stroke. *Neuroimage Clin*. 2015; 7: 771-781. doi: 10.1016/j.nicl.2015.03.007

22. Snow NJ, Peters S, Borich MR, et al. A reliability assessment of constrained spherical deconvolution-based diffusion-weighted magnetic resonance imaging in individuals with chronic stroke. *J Neurosci Methods*. 2015; 257: 109-120. doi: 10.1016/j.jneumeth.2015.09.025

23. Kristo G, Leemans A, Raemaekers M, Rutten GJ, de Gelder B, Ramsey NF. Reliability of two clinically relevant fiber pathways reconstructed with constrained spherical deconvolution. *Magn Reson Med*. 2013; 70(6): 1544-1556. doi: 10.1002/mrm.24602

24. Azadbakht H, Parkes LM, Haroon HA, et al. Validation of high-resolution tractography against in vivo tracing in the macaque visual cortex. *Cereb Cortex*. 2015; 25(11): 4299-309. doi: 10.1093/cercor/bhu326

25. Lerner A, Mogensen MA, Kim PE, Shiroishi MS, Hwang DH, Law M. Clinical applications of diffusion tensor imaging. *World Neurosurg*. 2014; 82(1-2): 96-109. doi: 10.1016/j.wneu.2013.07.083

26. Yao Y, Ulrich NH, Guggenberger R, Alzarhani YA, Bertalanffy H, Kollias SS. Quantification of corticospinal tracts with diffusion tensor imaging in brainstem surgery: prognostic value in 14 consecutive cases at 3t magnetic resonance imaging. *World Neurosurg*. 2015; 83(6): 1006-1014. doi: 10.1016/j.wneu.2015.01.045

27. Radmanesh A, Zamani AA, Whalen S, Tie Y, Suarez RO, Golby AJ. Comparison of seeding methods for visualization of the corticospinal tracts using single tensor tractography. *Clin Neurol Neurosurg*. 2015; 129: 44-49. doi: 10.1016/j.clineuro.2014.11.021

28. Birinyi PV, Bieser S, Reis M, et al. Impact of DTI tractography on surgical planning for resection of a pediatric pre-pontine neurenteric cyst: a case discussion and literature review. *Childs Nerv Syst*. 2015; 31(3): 457-463. doi: 10.1007/s00381-014-2587-0

ISSN 2473-0947 Open Journal http://dx.doi.org/10.17140/ROJ-1-e001

29. Mormina E, Longo M, Arrigo A, et al. MRI Tractography of corticospinal tract and arcuate fasciculus in high-grade gliomas performed by constrained spherical deconvolution: qualitative and quantitative analysis. *AJNR Am J Neuroradiol*. 2015; 36(10): 1853-1858. doi: 10.3174/ajnr.A4368

30. Jellison BJ, Field AS, Medow J, Lazar M, Salamat MS, Alexander AL. Diffusion tensor imaging of cerebral white matter: a pictorial review of physics, fiber tract anatomy, and tumor imaging patterns. *AJNR Am J Neuroradiol*. 2004; 25(3): 356-369.

31. Lu S, Ahn D, Johnson G, Cha S. Peritumoral diffusion tensor imaging of high-grade gliomas and metastatic brain tumors. *AJNR Am J Neuroradiol*. 2003; 24(5): 937-941.

32. Li Z, Peck KK, Brennan NP, et al. Diffusion tensor tractography of the arcuate fasciculus in patients with brain tumors: comparison between deterministic and probabilistic models. *J Biomed Sci Eng*. 2013; 6(2): 192-200.

33. Küpper H, Groeschel S, Alber M, Klose U, Schuhmann MU, Wilke M. Comparison of different tractography algorithms and validation by intraoperative stimulation in a child with a brain tumor. *Neuropediatrics*. 2015; 46(1): 72-75. doi: 10.1055/s-0034-1395346

34. Weiss C, Tursunova I, Neuschmelting V, et al. Improved nTMS- and DTI-derived CST tractography through anatomical ROI seeding on anterior pontine level compared to internal capsule. *Neuroimage Clin*. 2015; 7: 424-437. doi: 10.1016/j.nicl.2015.01.006

RADIOLOGY

Openventio PUBLISHERS

ISSN 2473-0947 Open Journal http://dx.doi.org/10.17140/ROJ-1-e002

Editorial

*Corresponding author
Alessandro Arrigo, MD
Department of Biomedical Sciences and Morphological and Functional Imaging
University of Messina
Via Consolare Valeria
1 Messina 98125, Italy
E-mail: alessandro.arrigo@hotmail.com

Volume 1 : Issue 1
Article Ref. #: 1000ROJ1e002

Article History
Received: January 22nd, 2016
Accepted: January 25th, 2016
Published: January 25th, 2016

Citation
Arrigo A, Calamuneri A, Mormina E. MRI investigation of optic radiations in human brain: new findings and technical considerations. *Radiol Open J*. 2016; 1(1): e6-e10. doi: 10.17140/ROJ-1-e002

MRI Investigation of Optic Radiations in Human Brain: New Findings and Technical Considerations

Alessandro Arrigo*, Alessandro Calamuneri and Enricomaria Mormina

Department of Biomedical Sciences and Morphological and Functional Images, University of Messina, Messina, Italy

KEYWORDS: Optic radiations; Tractography; Diffusion MRI; DTI; CSD.

ABBREVIATIONS: ORs: Optic Radiations; LGN: Lateral Geniculate Nucleus; DTI: Diffusion Tensor Imaging; MRI: Magnetic Resonance Imaging; HARDI: High Angular Resolution Diffusion-weighted Imaging; QBI: Q Ball Imaging; DSI: Diffusion Spectrum Imaging; CSD: Constrained Spherical Deconvolution; WM: White Matter; FA: Fractional Anisotropy.

Optic Radiations (ORs) are two white matter fiber bundles allowing direct connection between homolateral Lateral Geniculate Nucleus (LGN) and visual cortex. From the anatomical point of view, ORs are conventionally divided in three different portions, namely anterior, middle and posterior; the Meyer's loop represents the anterior portion, and it has been shown to be a bundle with a very high variability in human brain.[1-3] The latter aspect has to be taken into account when studying ORs in clinical and surgical contexts. Indeed, ORs represent eloquent white matter bundles often reconstructed by means of Magnetic Resonance Imaging (MRI) based approaches in order to assess their involvement by pathological conditions as well as to prevent post-surgical damages. Both these conditions can compromise visual function by causing, for instance, visual field deficits.[4,5] Schematic representation of ORs' bundles and common visual field deficits associated with ORs' lesions is shown in Figure 1.

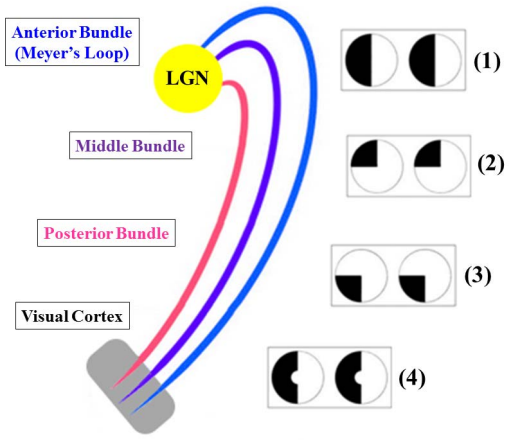

Figure 1: Schematic representation of ORs, from their origin from LGN (yellow) to visual cortex (grey) and common visual field deficits associated with ORs' lesions. Each bundle is colored separately. LGN's damage is followed by homonymous hemianopia (1). Lesions of the anterior bundle (blue) cause homonymous superior quadrantanopia (2) whereas damages of the posterior bundle (pink) are followed by homonymous inferior quadrantanopia (3). Middle bundle is shown in violet. Homonymous hemianopia with macular sparing can be seen after damages at visual cortex level (4).

ORs are largely studied by means of diffusion MRI based modelling techniques, such as Diffusion Tensor Imaging (DTI). These methods allow both qualitative evaluation

ISSN 2473-0947 Open Journal http://dx.doi.org/10.17140/ROJ-1-e002

of white matter bundles as well as quantitative analysis of several diffusion parameters, such as Fractional Anisotropy. The non-invasive investigation of ORs by means of diffusion MRI has provided several morphological information regarding ORs' connectivity. In particular, moving beyond well demonstrated link with V1 and V2,[6] direct connections with V3,[7] V4[8] and V5[8,9] have been recently shown. Functional implications of such connectivity include both primary visual signal elaboration as well as more complex functions; for example, direct connection with extra-striatal areas have been supposed to be implicated in the genesis of complex functional phenomena such as blindsight.[10] Moreover, other studies have hypothesized that such extra-striate connectivity might be the anatomical basis for the functional compensation performed after damages of striate visual cortex.[11]

In the context of tractographic driven investigation of ORs, several issues should be considered, especially if using conventional DTI. Indeed, ORs reconstruction might be potentially affected by well-known DTI limitations, such as partial volume effects.[12,13] Furthermore, several bundle-specific issues may compromise ORs tractographic reconstructions, e.g. complexity of ORs anatomical course as well as their relationship with other white matter bundles and brain structures.[1,2,8,14,15] From a technical perspective, several voxels with complex geometriesmay be involved, which are known to cause an inaccurate analysis when applying DTI model. These potential pitfalls raised several criticisms regarding reliability of tractographic findings regarding both ORs detection as well as extrastriate connectivity.[16] To overcome these limitations, other diffusion models have been tested to improve tractographic reconstructions, such as High Angular Resolution Diffusion-weighted Imaging (HARDI), Q Ball Imaging (QBI) and Diffusion Spectrum Imaging (DSI) algorithms. Although tractographic output provided by these approaches was found to outperform DTI based one, these algorithmsare however difficult to be applied in clinical contexts because they are really scanner demanding and time-consuming or they showed poor angular resolution.[17,18] From this point of view, Constrained Spherical Deconvolution (CSD)[18] has been found a powerful technique feasible in clinical settings. Recently, Arrigo and colleagues[8] have shown how the use of CSD model combined with probabilistic tractography provided robust ORs detection in healthy human brain. They were able to provide a more complete reconstruct of all ORs' portion, especially in case of Meyer's loop, justifying such result as being due to the higher angular resolution reached by CSD if compared to other models, as well asits ability to resolve voxels with complex fibers' configurations.[8,13,18] These voxels are indeed known to represent more than 90% of the total number in each brain, thus causing DTI reconstruction troubles for other eloquent bundles of White Matter (WM), such as corticospinal tract and arcuate fasciculus.[19] It is worthy to note that CSD has been already used to reconstruct ORs, providing accurate tracking of these white matter bundles and increasing reliability and details of ORs morphological profile.[20,21]

Arrigo et al[8] reinforced the hypothesis of ORs' extrastriate connectivity as well as their involvement in higher order visual functions. Moreover, direct LGN connection with V4 was shown for the first time in humans, reinforcing the findings provided by previous analyses performed in animals.[22,23] The comparative view of DTI based and CSD based ORs reconstructions is shown in Figure 2.

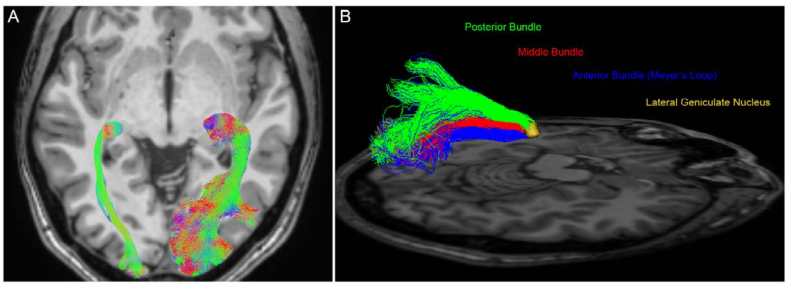

Figure 2: OR stractographic reconstruction in healthy human brain. (A) Axial view of DTI based (left side of the image) and CSD based (right side of the image) tractographic reconstructions showed a more complete ORs detection provided by CSD. Each bundle was colored according to its main diffusion direction. (B) Tridimensional sagittal view of CSD based reconstruction of left ORs. The use of CSD based tractography allowed a good detection of each ORs component. Anterior, middle and posterior ORs bundle, starting from LGN (yellow volume), were manually colored respectively in blue, red and green.

If benefits provided by CSD model are important in physiological contexts, they become extremely important in pathological ones, for instance during pre-surgical planning. Indeed, ORs are investigated both in patients with brain neoplasms as well as for surgical treatment of drug-resistant epilepsy, the latter consisting in the anterior temporal lobe resection.[3,24-27] Regarding brain neoplasms, many additional reconstruction's issues have been shown in these patients, which are caused by neoplasm's effects on diffusion signal; these potential pitfalls may be overcome by using more advanced diffusion signal modelling techniques, such as CSD, as previously reported in other studies.[28,29] Regarding pre-surgical planning of ORs, the use of CSD based tractography may increase definition of safety resection margins and it might have a good impact on post-surgical visual deficits.

From a quantitative point of view, the adoption of more advanced diffusion based approaches might have an impact on

evaluation of diffusion parameters. Indeed, when performing a tract based quantitative analysis, it should be taken into account that DTI would exclude voxels with complex geometry, since they often show Fractional Anisotropy (FA) values below a relative cut-off used for conventional tracking.[13] FA decrements can be found both in voxels with multiple orientations and in voxels involved by a pathological process.[30] The result of this DTI limitation is the loss of these voxels from the total count, determining an incomplete profiling of a given pathway. With respect to ORs, this issue may particularly affect Meyer's loop, which is known to be poorly detected when using DTI tractography; moreover, also other ORs' portions might be potentially affected due to the presence of crossing fibers.[8]

Performing diffusion parameters evaluation on the basis of CSD outcome may instead allow a more complete quantitative profile of ORs, thus allowing a better depiction of white matter integrity loss, like it has already been previously shown for other brain pathways.[13,28,29] A reliable quantitative evaluation is required for ORs evaluation in several diseases. Indeed, if ORs are directly involved in case, for instance,of neoplasms or multiple sclerosis, there exist a number of studies showing that that ORs can suffer from damages localized at other levels of the visual system as well, such as primitive optic nerve diseases. In particular, ORs diffusion parameters were found altered both in cases of glaucoma and optic neuritis.[31-33] These studies suggested that, although we are in presence of a localized damage, the entire visual system should be analyzed in order to assess possible negative effects on other visual structures. From this point of view, advanced methods such as CSD based tractography can be considered powerful tools for a deeper investigation of visual system damages.

This brief description attempted to summarize recent anatomical and physiological advances regarding ORs detection and analysis. Moreover, it showed how advanced diffusion signal modelling techniques may improve ORs' investigation both in healthy and pathological conditions, describing common as well as tract-specific diffusion issues. Furthermore, this study shows that the choice of diffusion model may have a huge impact both on qualitative and quantitative analysis of ORs.

CONFLICTS OF INTEREST

The authors declare that they have no conflicts of interest.

REFERENCES

1. Párraga RG, Ribas GC, Welling LC, et al. Microsurgical anatomyof the optic radiation and related fibers in 3-dimensional images. *Neurosurgery*. 2012; 71(Suppl 1): 160-171. doi: 10.1227/NEU.0b013e3182556fde

2. Pujari VB, Jimbo H, Dange N, et al. Fiber dissection of the visualpathways: analysis of the relationship of optic radiations to lateral ventricle: a cadaveric study. *Neurol India*. 2008; 56(2): 133-137. doi: 10.4103/0028-3886.41989

3. Nilsson D, Starck G, Ljungberg M, et al. Intersubjectvariability in the anterior extent of the optic radiation assessed by tractography. *Epilepsy Res*. 2007; 77(1): 11-16. doi: 10.1016/j.eplepsyres.2007.07.012

4. Longo D, Fauci A, Kasper D, et al. Harrison's Principles of Internal Medicine. 18th ed. McGraw-Hill Professional, 2011: 1 and 2.

5. Greenberg D, Aminoff M, Simon R. Clinical Neurology 8/E. McGraw-Hill Professional, 2012.

6. Baldwin MK, Kaskan PM, Zhang B, et al. Cortical and subcortical connections of V1 and V2 in early postnatal macaque monkeys. *J Comp Neurol*. 2012; 520(3): 544-569. doi: 10.1002/cne.22732

7. Alvarez I, Schwarzkopf DS, Clark CA. Extrastriate projections in human opticradiation revealed by fMRI-informed tractography. *Brain Struct Funct*. 2015; 220(5): 2519-2532. doi: 10.1007/s00429-014-0799-4

8. Arrigo A, Calamuneri A, Mormina EM, et al. New Insights in the optic radiations connectivity in the human brain. *Invest Ophthalmol Vis Sci*. 2016; 57(1): 1-5. doi: 10.1167/iovs.15-18082

9. Bridge H, Thomas O, Jbabdi S, Cowey A. Changes inconnectivity after visual cortical brain damage underlie alteredvisual function. *Brain*. 2008; 131: 1433-1444. doi: 10.1093/brain/awn063

10. Schmid MC, Mrowka SW, Turchi J, et al. Blindsight depends on the lateral geniculate nucleus. *Nature*. 2010; 466(7304): 373-377. doi: 10.1038/nature09179

ISSN 2473-0947 Open Journal http://dx.doi.org/10.17140/ROJ-1-e002

11. Bridge H, Hicks SL, Xie J, et al. Visual activation of extra-striatecortex in the absence of V1 activation. *Neuropsychologia*. 2010; 48: 4148-4154. doi: 10.1016/j.neuropsychologia.2010.10.022

12. Jones DK, Cercignani M. Twenty-five pitfalls in the analysis ofdiffusion MRI data. *NMR Biomed*. 2010; 23(7): 803-820. doi: 10.1002/nbm.1543

13. Farquharson S, Tournier JD, Calamante F, Fabinyi G, et al. White matter fiber tractography: whywe need to move beyond DTI. *J Neurosurg*. 2013; 118(6): 1367-1377. doi: 10.3171/2013.2.JNS121294

14. Kier EL, Staib LH, Davis LM, Bronen RA. MR imaging of thetemporal stem: anatomic dissection tractography of the uncinatefasciculus, inferior occipitofrontal fasciculus, and Meyer's loop of theoptic radiation. *AJNR Am J Neuroradiol*. 2004; 25(5): 677-691.

15. Peltier J, Verclytte S, Delmaire C, et al. Microsurgical anatomy of the temporal stem: clinical relevance and correlations with diffusion tensor imaging fiber tracking. *J Neurosurg*. 2010; 112(5): 1033-1038. doi: 10.3171/2009.6.JNS08132

16. Rabbo AF, Koch G, Lefevre C, Seizeur R. Direct geniculo-extrastriate pathways: a review of the literature. *Surg Radiol Anat*. 2015; 37: 891-899. doi: 10.1007/s00276-015-1450-7

17. Tournier JD, Calamante F, Connelly A. Robust determination of the fibre orientation distribution in diffusion MRI: nonnegativity constrained super-resolved spherical deconvolution. *Neuroimage*. 2007; 35: 1459-1472. doi: 10.1016/j.neuroimage.2007.02.016

18. Tournier JD, Yeh CH, Calamante F, et al. Resolving crossing fibres using constrained spherical deconvolution: validation using diffusion weighted imaging phantom data. *Neuroimage*. 2008; 42: 617-625. doi: 10.1016/j.neuroimage.2008.05.002

19. Jeurissen B, Leemans A, Tournier JD, et al. Investigating the prevalence of complex fiber configurationsin white matter tissue with diffusion magnetic resonance imaging. *Hum Brain Mapp*. 2013; 34: 2747-2766. doi: 10.1002/hbm.22099

20. Lim JC, Phal PM, Desmond PM, et al. Probabilistic MRI tractography of the optic radiation using constrained spherical deconvolution: a feasibility study. *PLoS One*. 2015; 10(3): e0118948. doi: 10.1371/journal.pone.0118948

21. Martínez-Heras E, Varriano F, Prčkovska V, et al. Improved framework for tractography reconstruction of the optic radiation. *PLoS One*. 2015; 10(9): e0137064. doi: 10.1371/journal.pone.0137064

22. Ferrera VP, Nealey TA, Maunsell JH. Responses in macaquevisual area V4 following inactivation of the parvocellular and magnocellular LGN pathways. *J Neurosci*. 1994; 14(4): 2080-2088.

23. Ungerleider LG, Galkin TW, Desimone R, Gattass R. Cortical connections of area V4 in the macaque. *Cereb Cortex*. 2008; 18: 477-499. doi: 10.1093/cercor/bhm061

24. Duncan JS. Imaging in the surgical treatment of epilepsy. *Nat Rev Neurol*. 2010; 6: 537-550. doi: 10.1038/nrneurol.2010.131

25. Winston GP, Daga P, Stretton J, et al. Optic radiation tractography and vision inanterior temporal lobe resection. *Ann Neurol*. 2012; 71(3): 334-341. doi: 10.1002/ana.22619

26. Piper RJ, Yoong MM, Kandasamy J, Chin RF. Application of diffusion tensor imaging and tractography of the optic radiation inanterior temporal lobe resection for epilepsy: a systematic review. *Clin Neurol Neurosurg*. 2014; 124C: 59-65. doi: 10.1016/j.clineuro.2014.06.013

27. Cho JM, Kim EH, Kim J, et al. Clinical use of diffusion tensor image-merged functional neuronavigationfor brain tumor surgeries: review of preoperative, intraoperative, andpostoperative data for 123 cases. *Yonsei Med J*. 2014; 55(5): 1303-1309. doi: 10.3349/ymj.2014.55.5.1303

28. Mormina E, Longo M, Arrigo A, et al. MRI tractography of corticospinal tract and arcuate fasciculus in high-grade gliomas performed by constrained spherical deconvolution: qualitative and quantitative analysis. *AJNR Am J Neuroradiol*. 2015; 36(10):

1853-1858. doi: 10.3174/ajnr.A4368

29. Arrigo A, Mormina E, Calamuneri A. The pre-surgical planning of brainneoplasms: from diffusion tensor imaging to more advanced approaches. *Radiol Open Journal.* 2015; 1(1): e1-e5.

30. Jellison BJ, Field AS, Medow J, et al. Diffusion tensor imaging of cerebral white matter: a pictorialreview of physics, fiber tract anatomy, and tumor imaging patterns. *AJNR Am J Neuroradiol*. 2004; 25(3): 356-369.

31. Dai H, Mu KT, Qi JP, et al. Assessment of lateral geniculate nucleus atrophywith 3T MR imaging and correlation with clinical stage of glaucoma. *AJNR Am J Neuroradiol*. 2011; 32(7): 1347-1353. doi: 10.3174/ajnr.A2486

32. El-Rafei A, Engelhorn T, Wärntges S, et al. Glaucoma classification based on histogram analysis of diffusion tensor imaging measures in the optic radiation. *ComputerAnalysis of Images and Patterns Lecture Notes in Computer Science*. 2011; 6854: 529-536.

33. Liu Y, Duan Y, He Y, et al. A tract-based diffusion study of cerebral white matter inneuromyelitis optica reveals widespread pathological alterations. *Mult Scler*. 2012; 18(7): 1013-1021. doi: 10.1177/1352458511431731

RADIOLOGY

Openventio PUBLISHERS

ISSN 2473-0947 Open Journal http://dx.doi.org/10.17140/ROJ-1-101

Review

*Corresponding author
Mohammed Inayathullah, PhD
Radiology-Molecular Imaging Program at Standford (MIPS)
Biomaterials and Advanced Drug Delivery (BioADD) Laboratory
Cardiovascular Pharmacology, Cardiovascular Institute
Stanford University School of Medicine
1050 Arastradero Road,
Building A, Room A163
Palo Alto, California, 94304, USA
Tel. 650-724-7710
Fax: 650-721-4651
E-mail: inayath@stanford.edu

Volume 1 : Issue 1
Article Ref. #: 1000ROJ1101

Article History
Received: November 17th, 2015
Accepted: December 10th, 2015
Published: December 11th, 2015

Citation
Parekh MB, Gurjarpadhye AA, Manoukian MAC, Dubnika A, Rajadas J, Inayathullah M. Recent developments in diffusion tensor imaging of brain. *Radiol Open J*. 2015; 1(1): 1-12. doi: 10.17140/ROJ-1-101

Recent Developments in Diffusion Tensor Imaging of Brain

Mansi Bharat Parekh[1,2], Abhijit Achyut Gurjarpadhye[1,3], Martin A.C. Manoukian[1,4], Arita Dubnika[1,5], Jayakumar Rajadas[1,6] and Mohammed Inayathullah[1,2,6*]

[1]Biomaterials and Advanced Drug Delivery Laboratory, Stanford University School of Medicine, Palo Alto, California, USA

[2]Department of Radiology, Stanford University School of Medicine, Stanford, California, USA

[3]Department of Dermatology, Stanford University School of Medicine, Stanford, California, USA

[4]University of California Davis School of Medicine, Sacramento, California, USA

[5]Riga Technical University, Faculty of Materials Science and Applied Chemistry, Institute of General Chemical Engineering, Rudolfs Cimdins Riga Biomaterials Innovations and Development Centre, Riga, Latvia

[6]Cardiovascular Pharmacology, Cardiovascular Institute, Stanford University School of Medicine, Stanford, California, USA

ABSTRACT

Magnetic Resonance Imaging (MRI) has come to be known as a unique radiological imaging modality because of its ability to perform tomographic imaging of body without the use of any harmful ionizing radiation. The radiologists use MRI to gain insight into the anatomy of organs, including the brain, while biomedical researchers explore the modality to gain better understanding of the brain structure and function. However, due to limited resolution and contrast, the conventional MRI fails to show the brain microstructure. Diffusion Tensor Imaging (DTI) harnesses the power of conventional MRI to deduce the diffusion dynamics of water molecules within the tissue and indirectly create a three-dimensional sketch of the brain anatomy. DTI enables visualization of brain tissue microstructure, which is extremely helpful in understanding various neuropathologies and neurodegenerative disorders. In this review, we briefly discuss the background and operating principles of DTI, followed by current trends in DTI applications for biomedical and clinical investigation of various brain diseases and disorders.

KEYWORDS: Brain imaging; Diffusion tensor imaging; Diffusion weighted imaging; Diffusion tensor tractography; Multiple sclerosis; Alzheimers; TBI.

ABBREVAITIONS: MRI: Magnetic Resonance Imaging; DTI: Diffusion Tensor Imaging; NMR: Nuclear Magnetic Resonance; MD: Mean Diffusivity; FA: Fractional Anisotropy; CSF: Cerebro-Spinal Fluid; WM: White Matter; GM: Gray Matter; FAD: Familial-AD; MCI: Mild Cognitive Impairment; EEG: Electro-encephalogram; TLE: Temporal Lobe Epilepsy; NAWM: Normal-Appearing White Matter; NAGM: Normal-Appearing Gray Matter; TBI: Traumatic Brain Injury; mTBI: mild TBI; CT: Computed Tomography; ATP: Adenosine tri-phosphate.

INTRODUCTION

Diffusion Weighted Imaging (DWI) is a powerful Magnetic Resonance Imaging (MRI) technique from a clinical standpoint, as the inherent rate of diffusion within various regions of the body can be measured. Stejskal and Tanner[1] first described the technique to measure water diffusion with Nuclear Magnetic Resonance (NMR) in 1965. Water molecules in the body encounter physical boundaries that impede their random displacement, i.e. molecules can hit a barrier and bounce back within the given diffusion time of the experiment. Thus, the

ISSN 2473-0947 Open Journal http://dx.doi.org/10.17140/ROJ-1-101

resultant signal may be higher than if the sample were under the same conditions but without barriers resulting in lower rates of diffusion than actuality.

DWI provides a powerful diagnostic tool as different diseases and disease states result in differential imbalances in local water content and diffusivity rates. Diffusion in the central nervous system may not be isotropic i.e. diffusion is not the same in all directions. Diffusion in white matter tracts is preferential in the direction of the fibers and very small perpendicular to the fiber. Thus white matter bundles within the brain exhibit high degrees of anisotropy within a given voxel. Signal intensity, in diffusion-weighted images of white matter, changes depending on the direction of the applied diffusion gradient, due to the preferential direction of diffusion within the fibers, thus offering a means of determining fiber orientation. Multiple DWI images acquired by applying differential pulses in different diffusion-sensitizing gradient directions can be fit to an apparent diffusion tensor model (Diffusion Tensor Imaging, (DTI)) which allows for the quantification of Mean Diffusivity (MD) and the anisotropy of water diffusion (Fractional Anisotropy, (FA)). For a rank-2 tensor fit, the diffusion tensor corresponds to a 3×3 square matrix in which the diagonal elements represent eigenvalues (λ_1, λ_2, and λ_3) corresponding to effective diffusion along the x, y and z axes,[2] while the off-diagonal elements represent correlations of the diffusivity between the three orthogonal axes. Each eigenvalue has an associated eigenvector, which defines the orientation of effective diffusion.

$$AD = \frac{(I_1^2 + I_2^2 + I_3^2)}{3} \quad (1)$$

$$FA = \sqrt{\frac{1}{2}} \frac{\sqrt{(\lambda_1 - \lambda_2)^2 + (\lambda_1 - \lambda_3)^2 + (\lambda_2 - \lambda_3)^2}}{\sqrt{\lambda_1^2 + \lambda_2^2 + \lambda_3^2}} \quad (2)$$

For regions with isotropic diffusion such as voxels with freely diffusing Cerebro-Spinal Fluid (CSF), the three eigenvalues have similar values. For regions with high anisotropy, such as white matter voxels, the eigenvalue in one direction is much greater than the magnitude in the other two directions (Figure 1). As diffusivity is higher along the length of the white matter, the primary eigenvector is representative

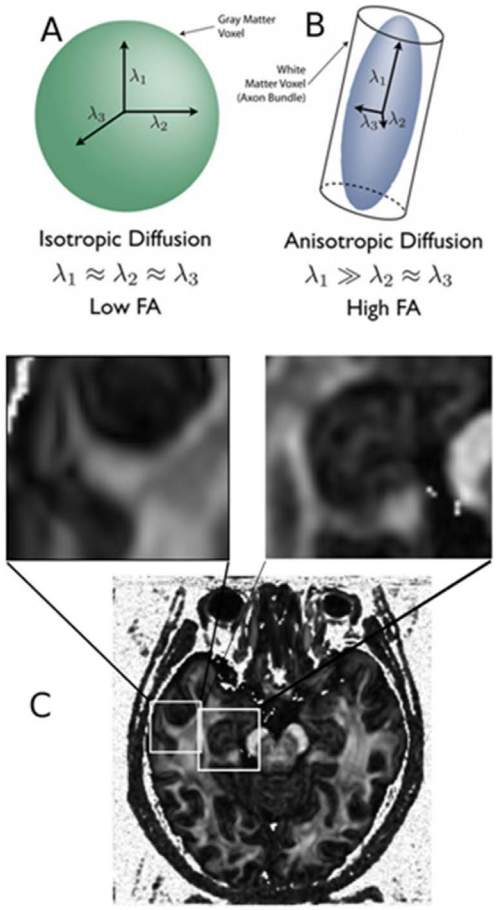

Figure 1: Diffusion tensor imaging. λ_1, λ_2 and λ_3 are the principle eigenvalues from the 3×3 matrix. Due to the tortuosity of various cell bodies and the extracellular matrix in grey matter regions, the values of λ_1, λ_2 and λ_3 are similar thus resulting in low FA values (A and C, top right inset). Due to the parallel arrangement of axons in white matter bundles, the value of λ_1 is usually much higher than λ_2 or λ_3, thus leading to higher FA values (B and C, top left inset).

ISSN 2473-0947 Open Journal http://dx.doi.org/10.17140/ROJ-1-101

of the average orientation of fibers within the voxel. In fact, this sensitivity, providing diffusion summary measures and tissue fiber orientation, has made DTI widely used as a clinical tool, especially in conditions where abnormalities in WM are expected and in healthy conditions.[3,4]

APPLICATIONS OF DTI OF BRAIN

Applications for Understanding Normal Neuronal Connectivity

Development of innovative and non-invasive methods for mapping brain connectivity at cellular and systems scale allow the acquisition of comprehensive whole-brain data sets from individual human subjects and their comparison with individual data on brain dynamics, cognition, behavior, and genetics. Information on the structural connectivity of human brain – human connectome, is fundamental for the formulation of mechanistic models of the network processes underlying human brain function.[5] DTI can provide insight into plastic/reactive changes in the microstructure and connectivity of white matter. In the human brain axons connect about 100 billion neurons and carry signals to, from, and within the brain and are the key factors that are studied on brain network connectivity.[6] The rate at which water molecules diffuse in the brain along a particular direction (the apparent diffusion co-efficient) can be measured *in vivo* by applying a diffusion sensitizing gradient in the direction of interest.[7]

By applying an orientation density function-based tractography method Hagmann et al measured the neuroconnectivity strength based on the number of fiber between any two brain regions.[8] Gong et al utilized diffusion tensor imaging deterministic tractography to construct the popularity-based anatomical network capturing the underlying connectivity pattern of human cerebral cortex in 80 young adults, comprising a streamline-like tractography method and statistics-based nonparametric sign test.[9] Bonilha et al have also shown that connectome mapping using DTI is reproducible (Figure 2).[10] In these studies network modeling was carried out considering that the brain network is a binary network ignoring the connectivity strength information among different brain regions.[8,9] To find the most probable trajectory between any two nodes Iturria-Medina et al used an iterative algorithm and applied anatomical connection probabilities to measure the connectivity strength between 90 cortical and subcortical brain gray matter areas.[11] Li et al extend the algorithm and model of the connectivity between different anatomical regions by performing tensor-based fast marching method, using the whole tensor field rather than just the principal directions.[6] But the newest connectome studies implement Brain X3 a virtual reality simulation cum data mining platform that is used to visualize, analyze and extract neuroscience data.[12]

Neuro-Degenerative and Neurological Disorders

Alzheimer's disease (AD): AD is the most common type of neurodegenerative dementia in aging population.[13] Early diagnosis is important for identifying candidate patients for the emerging therapies.[14] AD is characterized by loss of neurons, presence of senile plaques and neurofibrillary tangles that are found in the some neuroanatomical structures in the early course of the disease.[15] Anatomical MRI is used as a structural neuroimaging method for most of the AD studies and clinical trials; however DTI is a sensitive method to study microscopic White Matter (WM) changes that are not detectable with conventional MRI. DTI has been used for detecting regional WM alterations in AD followed by Gray Matter (GM) in the disease progression, which indicates that the cortical abnormalities are

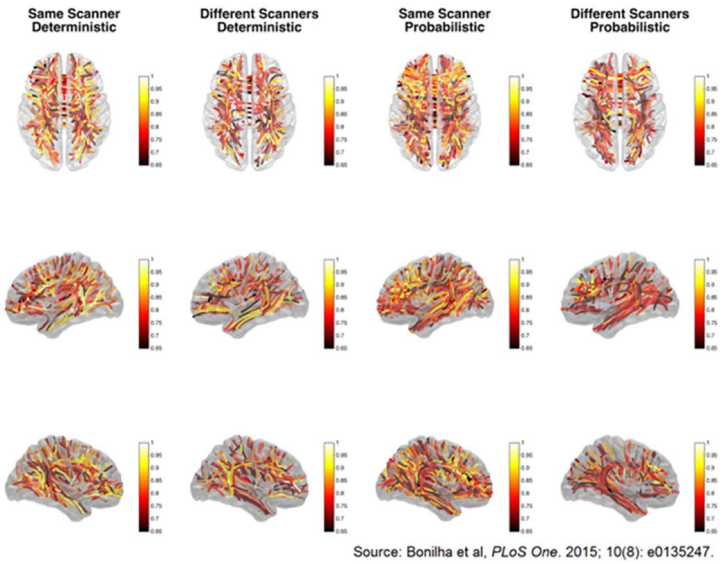

Source: Bonilha et al, *PLoS One*. 2015; 10(8): e0135247.

Figure 2: This figure demonstrates each connectome link represented by a line corresponding to the center of mass of the bundle of fibers associated with that link (estimated from deterministic tractography using DTI). Each link is color-coded based on its reproducibility per tractography approach and scanner usage. The color bars indicate the link-wise Intraclass Correlation Co-efficient showing that connectome mapping is largely reproducible using DTI. Reprinted from Bonilha et al.[10]

ISSN 2473-0947 Open Journal http://dx.doi.org/10.17140/ROJ-1-101

greater in posterior regions relative to anterior regions at the early stages of AD.[16,17] Several researchers have studied the loss of WM integrity in early AD[18-20] and in early Familial-AD (FAD).[21] Regional DTI has been shown to distinguish AD, Mild Cognitive Impairment (MCI) and normal aging[20,22-25] (Figure 3). DTI is being viewed as a crucial tool for AD diagnosis in recent years and has the potential to be used as a biomarker through analysis of various diffusion tensor metrics.[26,27]

Epilepsy: Spontaneous seizures that result in epilepsy may arise from synchronous firing of neurons from one region or a network of regions from various parts of the brain, which may be difficult to clinically isolate the seizure focus using traditional clinical modalities. DTI has proven fruitful in accomplishing this. Measurements in cerebral structural abnormalities and epilepsies, using DTI have shown significant changes in the mean rate of diffusion and the anisotropy of water motion.[28-32] The MD and FA which are invariant to image orientation were used to quantify aspects of water diffusion observed in cerebral tissue. These measures provide results similar to "stains" used in histological studies,[33,34] but allow them to be measured in intact tissue. Studies performed on experimentally induced SE showed reductions in ADC values in limbic as well as extra-limbic structures.[35-37] This decrease in ADC has been attributed to cytotoxic edema as excessive excitation leads to massive influx of sodium, chloride and calcium ions into the cells, leading to a net flow of water from the extra- to intracellular compartments, leading to an overall reduction in ADC.[38] Similar reductions in ADC, on the side of seizure focus deduced using Electro-encephalogram (EEG), have been observed in patients after prolonged seizures.[39] In focal epileptic regions, the mean rate of diffusion often increases and the anisotropy consistently decreases, reflecting neuronal loss, gliosis and structural disorganization.

A chronic elevation of diffusion rate is observed in Temporal Lobe Epilepsy (TLE) patients with hippocampal sclerosis, which has been attributed to neuronal necrosis, gliosis, and expanded extracellular space.[40] Using DTI, increased diffusion rate and a decreased diffusion anisotropy in the epileptic focus, compared to the contralateral region, was observed by Assaf et al[41] in patients with TLE. Similar studies using DTI have reported a reduction in diffusion anisotropy in the ipsilateral parahippocampal gyrus and fornix,[32,42] and also in extra-temporal white matter,[42] such as the internal capsule,[43] the external capsule,[44] the genu[43] and the splenium[44] of the corpus callosum (Figure 4). The reduction in diffusion anisotropy has been suggested to result from a loss of ordered structure, myelin degradation and lowered cell density.[32,43,45] Fiber tract maps generated from DTI measurements have also shown a reduction in tract volume of the fornix both pre[46] and post[47] resective surgery of the epileptogenic focus, as well as an increase in diffusion rate and a decrease in diffusion anisotropy in patients with unilateral TLE. Due to the ability of DTI to identify the epileptogenic focus, it has been utilized in surgical planning for the removal of the focus.[48,49]

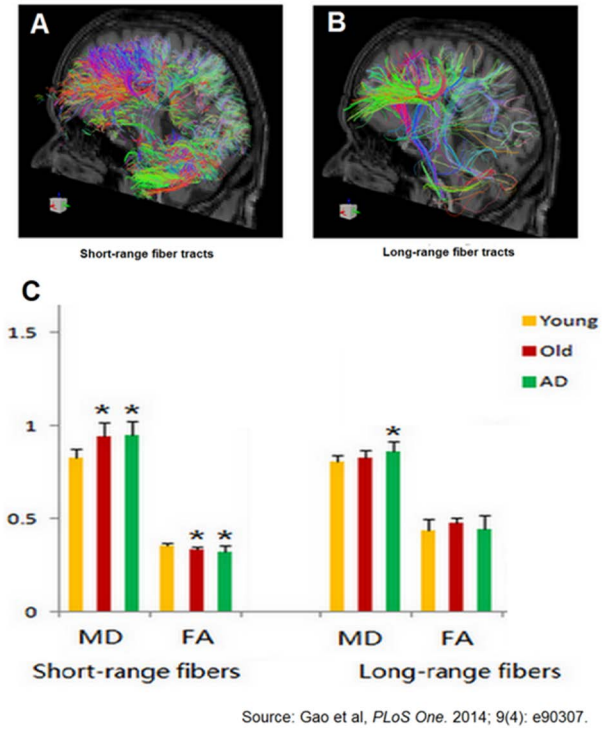

Source: Gao et al, *PLoS One*. 2014; 9(4): e90307.

Figure 3: Tractography demonstrations of ROI from fMRI data for (A), short-range fiber tracts, and for (B), long-range fiber tracts.(C), The MD, FA of short-range fiber tracts, long-range fiber tracts in three groups. Both MD and FA are useful in identifying differences between AD patients and normal (young and old). Reprinted from Gao et al.[25]

ISSN 2473-0947 Open Journal http://dx.doi.org/10.17140/ROJ-1-101

Multiple sclerosis (MS): MS is one of the most common neurodegenerative inflammatory diseases of the central nervous system, characterized by demyelination and axonal loss. The disease manifests through symptoms such as overall physical disability, imbalance of gait, sensory disturbance and cognitive dysfunction, the factor causing this disease are unknown.[50,51] MRI imaging plays an important role in early diagnosis of MS and in monitoring treatment efficacy; however, the technique shows low pathological specificity and low sensitivity to diffuse damage in Normal-Appearing White Matter (NAWM) and Normal-Appearing Gray Matter (NAGM).[52] In the recent years, DTI has proven to be an effective tool for detecting demyelination and tissue damage quantitatively.[53] Most commonly used DTI metrics, MD and FA measure overall water motion without any directionality, and the prevalence of diffusivity along one direction, respectively.[54] However, interpretation of these metrics for diagnosing specific pathologies in patients with MS is very complex. Several studies have been conducted to identify and establish correlation between pathophysiological conditions of specific anatomy and abnormalities in the MD and FA values.[55,56] Overall, the FA value, as it indicates the anisotropy of water diffusion along a specific direction, could serve as a reliable marker for estimating presence of plaques, lesions or overall microstructural changes in with the NAWM.[57] Additionally, Commowick et al suggested that instead of only replying on these scalar metrics such as MD and FA, demonstrated a framework that utilizes the whole diffusion tensor information to also in detect pathologies in the regions around existing legions, which allows an early detection of an extension of MS.[58]

Traumatic brain injury (TBI): Another important neurological disorder, TBI, affects 1.7 million people in the United States annually[59] and the clinical symptoms from TBI range from mild cognitive impairment to severe disability and neuroimaging plays a critical role in determining the course of therapy. Depending on the severity of the TBI, conventional MRI may or may not show abnormalities. In order to better diagnose cases of mild TBI (mTBI) (e.g. concussions), advanced neuroimaging techniques are being sought out. DTI is a potentially powerful research tool for investigating white matter pathology across a broad spectrum including mTBI. Various ROI-based studies have shown that DTI is sensitive in detecting group differences when comparing mTBI patients with healthy controls and suggest that DTI is sensitive to white matter changes[60-64] (Figure 5). Certain studies, such as by Miles et al have assessed the predictive value of DTI in determining cognitive function months after mTBI.[65] The observations from these various studies suggest that DTI is sensitive to white matter pathology following TBI, but all studies revealed substantial inter-individual differences in white matter integrity even among healthy controls.[61] These findings suggest that the specificity of such DTI abnormalities to mTBI is limited and illustrate well the problem of applying this technique to the examination of individual subjects and using DTI for any predictive value for future neurocognitive and neuropsychological changes.

Stroke: DTI can be used to evaluate damage in patients who have suffered an ischemic stroke due to the effects that the stroke has on the movement of fluids within the brain. DTI

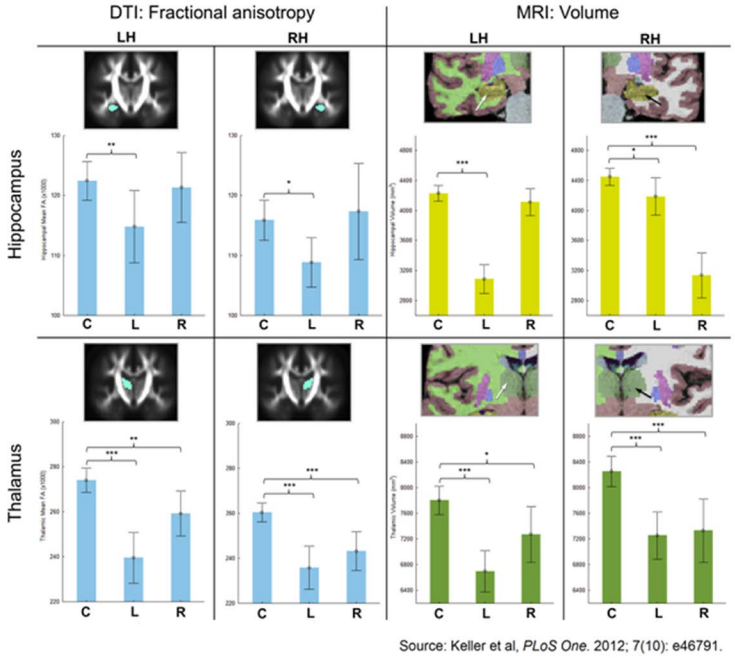

Figure 4: FA and volume alterations of the hippocampus and thalamus in patients with unilateral TLEhs relative to controls. The top row indicates mean (with 95% CI) FA (left) and volume (right) of the left and right hippocampus across controls (C), patients with left TLEhs (L) and patients with right TLEhs (R). The bottom row is the same for the thalamus. Structures are colour-coded: light blue for FA, yellow for hippocampal volume (as per standard Free Surfercolour classification) and dark green for thalamic volume (as per standard Free Surfercolour classification). FA values are the mean for each (corrected). **=significant at $p<0.01$ (corrected). ***=significant at p>0.001 (corrected). Reprinted from Keller et al.[42]

ISSN 2473-0947 Open Journal http://dx.doi.org/10.17140/ROJ-1-101

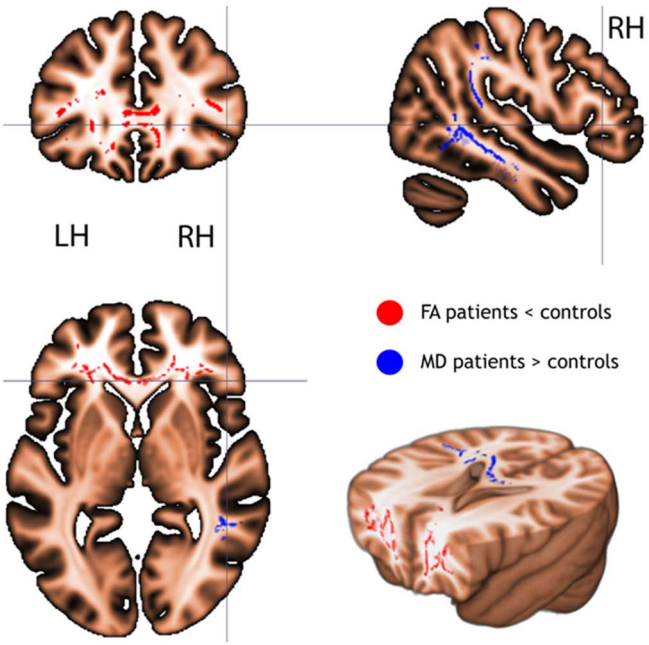

Source: Metting et al, *PLoS One*. 2013; 8(5): e64461.

Figure 5: Fractional anisotropy (FA) and mean diffusivity (MD) in mild traumatic brain injury. FA values are lower (red; P<0.08 - TFCE corrected) in mild traumatic brain injured patients compared to healthy control subjects and MD values are higher MD (blue; *P*<0.07- TFCE corrected). Reprinted from Metting et al.[64]

measurements have shown that FA within the white matter of the brain is significantly lower on the side of the brain that suffers an infraction when compared to the side of the brain that has not.[66,67] Thus, by looking at a complete map of FA within the brain of a patient that is suspected of having suffered a stroke, a physician is able to tell whether or not the stroke occurred, and if so, would be able to localize its point of action. It is important to note that DTI can detect the occurrence of a stroke much quicker after its occurrence than can conventional MRI imaging. Alterations in the diffusion characteristics resulting from an ischemic event can be detected within hours of the event's occurrence using DTI, whereas it could take days for the same stroke to be detectable by conventional MRI,[68] This makes DTI an indispensable tool in the diagnosis of ischemic strokes, as a quicker diagnosis can lead to a quicker physician response time, which has tremendous impacts on long term patient outcomes.

In addition to identifying the area of the brain impacted by an ischemic stroke, DTI can also be used to identify areas of the brain and spinal tract distal to the location of the stroke that are also affected. The break-down of myelin sheaths and disintegration of axonal microfilaments of neurons downstream of the site of the stroke, also known as Wallerian degeneration, can be detected due to its negative anisotropic effects. Though capable of detection rapidly *via* DTI, Wallerian degeneration is difficult to identify with conventional MR imaging techniques for many weeks after the occurrence of the stroke.[69,70] It is therefore advisable that physicians thoroughly examine stroke patients using DTI techniques to find areas that are affected by Wallerian degeneration, thereby increasing the chances of discovery, treatment, and that the patient has an improved recovery process.

Edema

Cytotoxic edema: Cytotoxic edema results from a decrease in the function of the Adenosine tri-phosphate (ATP)-dependent sodium/potassium pumps (Na^+/K^+ ATPases) located on the surface of cells within the brain. This decrease in Na^+/K^+ ATPase activity is caused by oxygen deprivation that prevents oxidative phosphorylation from occurring, and thereby inhibiting ATP production. Hypoxemia can be caused by such events as a stroke, hemorrhage, or embolism. Although the mitochondria of the brain have mechanisms in place to cope with hypoxemia, such as pathways that include hypoxia-inducible factor 1 and succinate dehydrogenase, these mechanisms can only do so much before ATP levels drop to pathological levels.[71] Once ATP levels fall, the Na^+/K^+ ATPases lose the capacity to translocate sodium out of the cell, leading to the buildup of intracellular sodium levels. This sodium buildup causes the creation of an osmotic gradient that promotes the diffusion of water into the cell, leading to a rapid and intense increase in intracellular volume. Cytotoxic edema has been shown to affect both the white and the grey matter of the brain, causing generalized swelling and widespread damage.[72] The accumulation of water molecules within the intracellular spaces severely impedes their ability to flow freely. Though water molecules can diffuse through the plasma membranes of the cells, doing so greatly slows their velocity,

ISSN 2473-0947 Open Journal http://dx.doi.org/10.17140/ROJ-1-101

leading to a net decrease in diffusivity within the area of the brain affected by the cytotoxic edema. When imaged with different modalities, cytotoxic edema presents as a decrease in attenuation *via* Computed Tomography (CT) scan, hyperintensity *via* MRI, and a decreased diffusivity by DTI. Though the readings from CT and MR imaging are found in all cases of edema, it is only DTI which is able to differentiate between subtypes of edema, and assist with the definite diagnosis of cytotoxic edema. Using this phenomenon DTI detection of cytotoxic edema can be used as an early warning for acute stroke, acute diffuse axonal injury, and acute contusion.[73,74]

Vasogenic edema: Vasogenic edema results from a breakdown of the blood brain barrier that can be caused by local factors such as neoplasm or traumatic brain injury, or from chronic damage caused by lead encephalopathy or malignant hypertension.[73] Thus, vasogenic edema is an extracellular accumulation of fluid, as opposed to the intracellular accumulation seen in cytotoxic edema. Vasogenic edema presentation mimics cytotoxic edema when using CT and MRI imaging, in that both present with decreased attenuation *via* CT and hyperintensity *via* MRI. However, when using DTI, vasogenic edema presents with an increased diffusivity, as opposed to the decreased diffusivity shown by cytotoxic edema.[73,75] This is because the water molecules within the extracellular space can move more freely than the water molecules that are confined within the intracellular space by plasma membranes. Thus, it is important to note that DTI is able to differentiate cytotoxic edema from vasogenic edema, whereas CT and conventional MRI cannot.

It is important that the physician is able to differentiate whether the patient is suffering from cytotoxic edema, vasogenic edema, or a combination of the two[76] (Figure 6) so that the correct intervention can be applied as necessary. However, it is often the case that cytotoxic and vasogenic edema occur in parallel.[77] For example, following an ischemic attack, cytotoxic edema occurs immediately due to local hypoxmia and a slow-down of the Na^+/K^+ ATPase pumps. Following the initial intracellular fluid accumulation, blood brain barrier breakdown occurs, leading to concurrent vasogenic edema.[78] Though cytotoxic edema does not currently have a widely accepted therapy, vasogenic edema is generally treated with corticosteroids, particularly when associated with neoplasms, and to a lesser extent when associated with abscesses. In cases where it is not responsive to corticosteroids, vasogenic edema can also be treated with osmotherapy.[72]

LIMITATIONS OF DTI

Despite a plethora of studies having employed DTI to study normal and abnormal brain integrity, the acquisition and approaches of DTI analyses have been quite variable. Though the connectome project is making great strides in the right direction, no common frame of reference for the comparison of findings between studies. For example, some studies use ADC as a measure of white matter integrity while others use FA. Additionally others use radial diffusivity and axial integrity to help determine the contribution of various types of pathologies. While some studies use ROI-based analyses to test specific

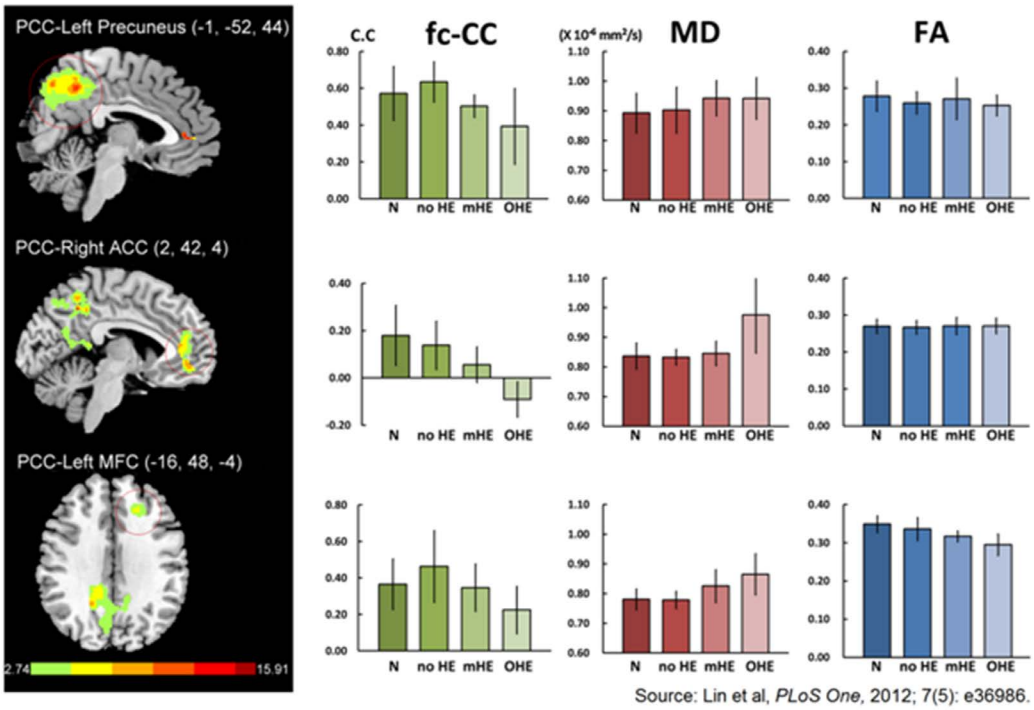

Figure 6: Connectivity of Default-Mode Network Is Associated with Cerebral Edema in Hepatic Encephalopathy. Differences of default model network between health subjects and liver cirrhosis and their corresponding MD and FA values. There were three biggest cluster areas in the PCC functional connectivity map, including the left precuneus, right ACC and left middle frontal cortex (MFC). MANCOVA revealed significant fc-CC [F=4.415, p=0.000] and MD [F=3.944, p=0.000] differences among the four groups, but not in FA [F=0.859, p=0.063]. Reprinted from Lin et al.[76]

anatomic hypotheses, some studies employ hypothesis-free analyses of the whole brain and apply one of the several methods of correction for multiple unplanned comparisons to identify significant findings. One of the main technical issues is the lack of a large normative database. Normative databases are needed to interpret individual (i.e. single subject or single patient) FA, ADC, or other values for clinical purposes. In the absence of normative databases of these sorts, each institution at which DTI is performed is left to develop and employ their own normative data when attempting to interpret group or single-subject DTI data. The size and normality of subjects included in these databases is highly variable between institutions, rendering the interpretation of any individual DTI result as normal or abnormal based on comparison to local normative data preliminary at best. The DTI literature available is affected by the heterogeneity of injury captured under the various disorders; heterogeneity in the time after injury at which persons have been studied with DTI; and the lack of a standard, accepted method for acquiring, analyzing, and interpreting DTI data. In light of these limitations, there is need to create a large normative database for DTI to be utilized at its potential.

CONCLUSIONS AND FUTURE POTENTIALS

DTI, as we discussed in this review has proved to be an important tool for diagnosing various pathologies of the brain. In addition to brain imaging, DTI is being actively developed for diagnosis of spinal cord pathologies,[79-81] and optics nerve damage.[82,83] Additionally, while DTI in infants and toddlers is challenging, the technique shows great potential for understanding and mapping brain development. Technological improvements in MR imaging could soon allow researchers to gather artifact-free data more reliably, which could significantly aid in understanding brain development in infants and toddlers. Biomarkers could be created for prediction and early detection of neurodegenerative disorders, which will allow researchers to develop better therapeutic approaches and surgeons to design better treatment strategies. While it may seem too ambitious, set of normal FA and MD values could be derived by conducting DTI of larger population – in a similar way that "normal" blood pressure values of 120/80 mm Hg were determined. We acknowledge, however that such task also requires standardization of imaging, post-processing and data analysis procedures as these factor may affect the quantification of DTI parameters. In summary, DTI modality shows an enormous potential to be a versatile tool for biomedical research and clinical applications.

CONFLICTS OF INTEREST

The authors declare that they have no conflicts of interest.

ACKNOWLEDGEMENTS

Dr. Michael Zeineh of the Stanford Department of Radiology provided Figure 1. The project described was supported by the National Center for Research Resources and the National Center for Advocacy Translational Sciences, National Institutes of Health, through UL1 TR000093 (formerly UL1 RR025744) and SPARK, Spectrum - the Stanford Center for Clinical and Translational Research and Education; the Stanford NIH/NCCR Clinical Translational Science Award grant number TL1 RR025742, and author AD was supported by the Baltic-American Freedom Foundation.

REFERENCES

1. Stejskal EO, Tanner JE. Spin diffusion measurements: spin echoes in the presence of a time-dependent field gradient. *Journal of Chemical Physics.* 1965; 42(1): 288-292. doi: 10.1063/1.1695690

2. Basser PJ, Mattiello J, Lebihan D. MR diffusion tensor spectroscopy and imaging. *Biophys J.* 1994; 66(1): 259-267. doi: 10.1016/S0006-3495(94)80775-1

3. Thomason ME, Thompson PM. Diffusion imaging, white matter, and psychopathology. *Annu Rev Clin Psychol.* 2011; 7: 63-85. doi: 10.1146/annurev-clinpsy-032210-104507

4. Mori S, Zhang J. Principles of diffusion tensor imaging and its applications to basic neuroscience research. *Neuron.* 2006; 51(5): 527-539. doi: 10.1016/j.neuron.2006.08.012

5. Sporns O. The human connectome: a complex network. *Ann N Y Acad Sci.* 2011; 1224: 109-125. doi: 10.1111/j.1749-6632.2010.05888.x

6. Li H, Xue Z, Cui K, Wong ST. Diffusion tensor-based fast marching for modeling human brain connectivity network. *Comput Med Imaging Graph.* 2011; 35(3): 167-178.

7. Steel RM, Bastin ME, Mcconnell S, et al. Diffusion tensor imaging (DTI) and proton magnetic resonance spectroscopy (1H MRS) in schizophrenic subjects and normal controls. *Psychiatry Res.* 2001; 106(3): 161-170. doi: 10.1016/j.compmedimag.2010.07.008

8. Hagmann P, Kurant M, Gigandet X, et al. Mapping human whole-brain structural networks with diffusion MRI. *PLoS One.* 2007; 2(7): e597. doi: 10.1371/journal.pone.0000597

9. Gong GL, He Y, Concha L, et al. Mapping anatomical connectivity patterns of human cerebral cortex using in vivo diffusion tensor imaging tractography. *Cerebral Cortex.* 2009; 19(3): 524-536. doi: 10.1093/cercor/bhn102

10. Bonilha L, Gleichgerrcht E, Fridriksson J, et al. Reproducibility of the structural brain connectome derived from diffusion tensor imaging. *PLoS One.* 2015; 10(8): e0135247. doi: 10.1371/journal.pone.0135247

11. Iturria-Medina Y, Sotero RC, Canales-Rodriguez EJ,

Aleman-Gomez Y, Melie-Garcia L. Studying the human brain anatomical network via diffusion-weighted MRI and Graph Theory. *Neuroimage.* 2008; 40(3): 1064-1076. doi: 10.1016/j.neuroimage.2007.10.060

12. Arsiwalla XD, Dalmazzo D, Zucca R, et al. Connectomics to semantomics: addressing the brain's big data challenge. *Inns Conference on Big Data 2015 Program.* 2015; 53: 48-55. doi: 10.1016/j.procs.2015.07.278

13. Holtzman DM, Morris JC, Goate AM. Alzheimer's disease: the challenge of the second century. *Sci Transl Med.* 2011; 3(77): 77sr71. doi: 10.1126/scitranslmed.3002369

14. Dubois B, Feldman HH, Jacova C, et al. Research criteria for the diagnosis of Alzheimer's disease: revising the NINCDS-ADRDA criteria. *Lancet Neurol.* 2007; 6(8): 734-746. doi: 10.1016/S1474-4422(07)70178-3

15. Goedert M, Spillantini MG. A century of Alzheimer's disease. *Science.* 2006; 314(5800): 777-781. doi: 10.1126/science.1132814

16. Arnold SE, Hyman BT, Flory J, Damasio AR, Van Hoesen GW. The topographical and neuroanatomical distribution of neurofibrillary tangles and neuritic plaques in the cerebral cortex of patients with Alzheimer's disease. *Cerebral Cortex.* 1991; 1(1): 103-116. doi: 10.1093/cercor/1.1.103

17. Braak H, Braak E. Staging of Alzheimer's disease-related neurofibrillary changes. *Neurobiol Aging.* 1995; 16(3): 271-278; discussion 278-284. doi: 10.1016/0197-4580(95)00021-6

18. Rose SE, Chen F, Chalk JB, et al. Loss of connectivity in Alzheimer's disease: an evaluation of white matter tract integrity with colour coded MR diffusion tensor imaging. *J Neurol Neurosurg Psychiatry.* 2000; 69(4): 528-530. doi: 10.1136/jnnp.69.4.528

19. Medina DA, Gaviria M. Diffusion tensor imaging investigations in Alzheimer's disease: the resurgence of white matter compromise in the cortical dysfunction of the aging brain. *Neuropsychiatr Dis Treat.* 2008; 4(4): 737-742. doi: 10.2147/NDT.S3381

20. Fu JL, Liu Y, Li YM, Chang C, Li WB. Use of diffusion tensor imaging for evaluating changes in the microstructural integrity of white matter over 3 years in patients with amnesic-type mild cognitive impairment converting to Alzheimer's disease. *J Neuroimaging.* 2014; 24(4): 343-348. doi: 10.1111/jon.12061

21. Ringman JM, O'neill J, Geschwind D, et al. Diffusion tensor imaging in preclinical and presymptomatic carriers of familial Alzheimer's disease mutations. *Brain.* 2007; 130(Pt 7): 1767-1776. doi: 10.1093/brain/awm102

22. Nir TM, Jahanshad N, Villalon-Reina JE, et al. Effectiveness of regional DTI measures in distinguishing Alzheimer's disease, MCI, and normal aging. *Neuroimage Clin.* 2013; 3: 180-195. doi: 10.1016/j.nicl.2013.07.006

23. Stebbins GT, Murphy CM. Diffusion tensor imaging in Alzheimer's disease and mild cognitive impairment. *Behav Neurol.* 2009; 21(1): 39-49. doi: 10.3233/BEN-2009-0234

24. Chua TC, Wen W, Slavin MJ, Sachdev PS. Diffusion tensor imaging in mild cognitive impairment and Alzheimer's disease: a review. *Curr Opin Neurol.* 2008; 21(1): 83-92. doi: 10.1097/WCO.0b013e3282f4594b

25. Gao J, Cheung RT, Chan YS, et al. The relevance of short-range fibers to cognitive efficiency and brain activation in aging and dementia. *PLoS One.* 2014; 9(4): e90307. doi: 10.1371/journal.pone.0090307

26. Acosta-Cabronero J, Alley S, Williams GB, Pengas G, Nestor PJ. Diffusion tensor metrics as biomarkers in Alzheimer's disease. *PLoS One.* 2012; 7(11): e49072. doi: 10.1371/journal.pone.0049072

27. Clerx L, Visser PJ, Verhey F, Aalten P. New MRI markers for Alzheimer's disease: a meta-analysis of diffusion tensor imaging and a comparison with medial temporal lobe measurements. *J Alzheimers Dis.* 2012; 29(2): 405-429. doi: 10.3233/JAD-2011-110797

28. Wieshmann UC, Clark CA, Symms MR, et al. Reduced anisotropy of water diffusion in structural cerebral abnormalities demonstrated with diffusion tensor imaging. *Magn Reson Imaging.* 1999; 17(9): 1269-1274. doi: 10.1016/S0730-725X(99)00082-X

29. Eriksson SH, Stepney A, Symms MR, et al. Ultra-fast low-angle rapid acquisition and relaxation enhancement (UFLARE) in patients with epilepsy. *Neuroradiology.* 2001; 43(12): 1040-1045.

30. Rugg-Gunn FJ, Eriksson SH, Symms MR, Barker GJ, Duncan JS. Diffusion tensor imaging of cryptogenic and acquired partial epilepsies. *Brain.* 2001; 124(Pt 3): 627-636. doi: 10.1093/brain/124.3.627

31. Briellmann RS, Mitchell LA, Waites AB, et al. Correlation between language organization and diffusion tensor abnormalities in refractory partial epilepsy. *Epilepsia.* 2003; 44(12): 1541-1545. doi: 10.1111/j.0013-9580.2003.19403.x

32. Focke NK, Yogarajah M, Bonelli SB, et al. Voxel-based diffusion tensor imaging in patients with mesial temporal lobe epilepsy and hippocampal sclerosis. *Neuroimage.* 2008; 40(2): 728-737. doi: 10.1016/j.neuroimage.2007.12.031

33. Basser PJ. Inferring microstructural features and the physiological state of tissues from diffusion-weighted images. *NMR in Biomedicine.* 1995; 8(7-8): 333-344.

34. Basser PJ. New histological and physiological stains derived from diffusion-tensor MR images. *Ann N Y Acad Sci.* 1997; 820: 123-138. doi: 10.1111/j.1749-6632.1997.tb46192.x

35. Zhong J, Petroff OA, Prichard JW, Gore JC. Changes in water diffusion and relaxation properties of rat cerebrum during status epilepticus. *Magn Reson Med.* 1993; 30(2): 241-246. doi: 10.1002/mrm.1910300214

36. Nakasu Y, Nakasu S, Kizuki H, et al. Changes in water diffusion of rat limbic system during status epilepticus elicited by kainate. *Psychiatry Clin Neurosci.* 1995; 49(3): S228-S230. doi: 10.1111/j.1440-1819.1995.tb02184.x

37. Parekh MB, Carney PR, Sepulveda H, et al. Early MR diffusion and relaxation changes in the parahippocampal gyrus precede the onset of spontaneous seizures in an animal model of chronic limbic epilepsy. *Exp Neurol.* 2010; 224(1): 258-270. doi: 10.1016/j.expneurol.2010.03.031

38. Moseley ME, Wendland MF, Kucharczyk J. Magnetic resonance imaging of diffusion and perfusion. *Top Magn Reson Imaging.* 1991; 3(3): 50-67.

39. Parmar H, Lim SH, Tan NC, Lim CC. Acute symptomatic seizures and hippocampus damage: DWI and MRS findings. *Neurology.* 2006; 66(11): 1732-1735.

40. Hugg JW, Butterworth EJ, Kuzniecky RI. Diffusion mapping applied to mesial temporal lobe epilepsy: preliminary observations. *Neurology.* 1999; 53(1): 173-176. doi: 10.1212/WNL.53.1.173

41. Assaf BA, Mohamed FB, Abou-Khaled KJ, et al. Diffusion tensor imaging of the hippocampal formation in temporal lobe epilepsy. *AJNR Am J Neuroradiol.* 2003; 24(9): 1857-1862.

42. Keller SS, Schoene-Bake JC, Gerdes JS, Weber B, Deppe M. Concomitant fractional anisotropy and volumetric abnormalities in temporal lobe epilepsy: cross-sectional evidence for progressive neurologic injury. *PLoS One.* 2012; 7(10): e46791. doi: 10.1371/journal.pone.0046791

43. Gross DW, Concha L, Beaulieu C. Extratemporal white matter abnormalities in mesial temporal lobe epilepsy demonstrated with diffusion tensor imaging. *Epilepsia.* 2006; 47(8): 1360-1363. doi: 10.1111/j.1528-1167.2006.00603.x

44. Arfanakis K, Hermann BP, Rogers BP, et al. Diffusion tensor MRI in temporal lobe epilepsy. *Magn Reson Imaging.* 2002; 20(7): 511-519. doi: 10.1016/S0730-725X(02)00509-X

45. Kim S, Pickup S, Hsu O, Poptani H. Diffusion tensor MRI in rat models of invasive and well-demarcated brain tumors. *NMR Biomed.* 2008; 21(3): 208-216.

46. Concha L, Beaulieu C, Gross DW. Bilateral limbic diffusion abnormalities in unilateral temporal lobe epilepsy. *Ann Neurol.* 2005; 57(2): 188-196. doi: 10.1002/ana.20334

47. Concha L, Beaulieu C, Wheatley BM, Gross DW. Bilateral white matter diffusion changes persist after epilepsy surgery. *Epilepsia.* 2007; 48(5): 931-940. doi: 10.1111/j.1528-1167.2007.01006

48. Richardson MP. Epilepsy and surgical mapping. *Br Med Bull.* 2003; 65: 179-192. doi: 10.1093/bmb/65.1.179

49. Zhang J, Liu W, Chen H, et al. Multimodal neuroimaging in presurgical evaluation of drug-resistant epilepsy. *Neuroimage Clin.* 2014; 4: 35-44. doi: 10.1016/j.nicl.2013.10.017

50. Bhatia R, Bali P, Chaudhari RM. Epidemiology and genetic aspects of multiple sclerosis in India. *Ann Indian Acad Neurol.* 2015; 18(Suppl 1): S6-S10. doi: 10.4103/0972-2327.164814

51. Shah P. Symptomatic management in multiple sclerosis. *Ann Indian Acad Neurol.* 2015; 18(Suppl 1): S35-S42. doi: 10.4103/0972-2327.164827

52. Meng X, Wang Q, Hou J, et al. Diffusion tensor imaging of normal-appearing white matter in unilateral cerebral arterial occlusive disease. *J Magn Reson Imaging.* 2013; 38(3): 650-654. doi: 10.1002/jmri.24004

53. Miller TR, Mohan S, Choudhri AF, Gandhi D, Jindal G. Advances in multiple sclerosis and its variants: conventional and newer imaging techniques. *Radiol Clin North Am.* 2014; 52(2): 321-336. doi: 10.1016/j.rcl.2013.11.011

54. Pierpaoli C, Jezzard P, Basser PJ, Barnett A, Di Chiro G. Diffusion tensor MR imaging of the human brain. *Radiology.* 1996; 201(3): 637-648. doi: 10.1148/radiology.201.3.8939209

55. Liu Y, Duan Y, He Y, et al. Whole brain white matter changes revealed by multiple diffusion metrics in multiple sclerosis: a TBSS study. *Eur J Radiol.* 2012; 81(10): 2826-2832. doi: 10.1016/j.ejrad.2011.11.022

56. Calabrese M, Rinaldi F, Seppi D, et al. Cortical diffusion-tensor imaging abnormalities in multiple sclerosis: a 3-year longitudinal study. *Radiology.* 2011; 261(3): 891-898. doi: 10.1148/radiol.11110195

57. Banaszek A, Bladowska J, Pokryszko-Dragan A, Podemski R, Sasiadek MJ. Evaluation of the degradation of the selected projectile, commissural and association white matter tracts within normal appearing white matter in patients with multiple

sclerosis using diffusion tensor mr imaging-a preliminary study. *Pol J Radiol.* 2015; 80: 457-463. doi: 10.12659/PJR.894661

58. Commowick O, Fillard P, Clatz O, Warfield SK. Detection of DTI white matter abnormalities in multiple sclerosis patients. *Med Image Comput Comput Assist Interv.* 2008; 11(Pt 1): 975-982.

59. Faul M, Xu L, Wald MM, Coronado VG. Traumatic brain injury in the United States: emergency department visits, hospitalizations, and deaths 2002-2006, Centers for Disease Control and Prevention, National Center for Injury Prevention and Control: Atlanta (GA), 2010.

60. Inglese M, Makani S, Johnson G, et al. Diffuse axonal injury in mild traumatic brain injury: a diffusion tensor imaging study. *J Neurosurg.* 2005; 103(2): 298-303. Available at: http://thejns.org/doi/abs/10.3171/jns.2005.103.2.0298?url_ver=Z39.88-2003&rfr_id=ori%3Arid%3Acrossref.org&rfr_dat=cr_pub%3Dpubmed&

61. Kraus MF, Susmaras T, Caughlin BP, et al. White matter integrity and cognition in chronic traumatic brain injury: a diffusion tensor imaging study. *Brain.* 2007; 130(Pt 10): 2508-2519. doi: 10.1093/brain/awm216

62. Geary EK, Kraus MF, Pliskin NH, Little DM. Verbal learning differences in chronic mild traumatic brain injury. *J Int Neuropsychol Soc.* 2010; 16(3): 506-516. doi: 10.1017/S135561771000010X

63. Rutgers DR, Fillard P, Paradot G, et al. Diffusion tensor imaging characteristics of the corpus callosum in mild, moderate, and severe traumatic brain injury. *AJNR Am J Neuroradiol.* 2008; 29(9): 1730-1735. doi: 10.3174/ajnr.A1213

64. Metting Z, Cerliani L, Rodiger LA, Van Der Naalt J. Pathophysiological concepts in mild traumatic brain injury: diffusion tensor imaging related to acute perfusion CT imaging. *PLoS One.* 2013; 8(5): e64461. doi: 10.1371/journal.pone.0064461

65. Miles L, Grossman RI, Johnson G, et al. Short-term DTI predictors of cognitive dysfunction in mild traumatic brain injury. *Brain Inj.* 2008; 22(2): 115-122. doi: 10.1080/02699050801888816

66. Chen Z, Ni P, Zhang J, et al. Evaluating ischemic stroke with diffusion tensor imaging. *Neurol Res.* 2008; 30(7): 720-726. doi: 10.1179/174313208X297968

67. Mukherjee P. Diffusion tensor imaging and fiber tractography in acute stroke. *Neuroimaging Clin N Am.* 2005; 15(3): 655-665, xii.

68. Neil JJ. Diffusion imaging concepts for clinicians. *J Magn Reson Imaging.* 2008; 27(1): 1-7. doi: 10.1002/jmri.21087

69. Werring DJ, Toosy AT, Clark CA, et al. Diffusion tensor imaging can detect and quantify corticospinal tract degeneration after stroke. *J Neurol Neurosurg Psychiatry.* 2000; 69(2): 269-272. doi: 10.1136/jnnp.69.2.269

70. Ni J, Li ML, Yao M, Cui LY. Early corticospinal tract Wallerian degeneration on diffusion-weighted MR imaging after adult stroke: three cases report. *Clin Neurol Neurosurg.* 2013; 115(7): 1164-1166. doi: 10.1016/j.clineuro.2012.09.027

71. Lukyanova LD, Kirova YI. Mitochondria-controlled signaling mechanisms of brain protection in hypoxia. *Front Neurosci.* 2015; 9: 320. doi: 10.3389/fnins.2015.00320

72. Mariano G, Fink M, Hoffman C, Rosengart A. Intracranial pressure: monitoring and management in principles of critical care, McGraw-Hill Education LLC,: New York, NY, 2015: 1 online resource.

73. Ropper AH, Samuels MA, Klein J. Intracranial neoplasms and paraneoplastic disorders. In: Ropper AH, Samuels MA, Klein J, eds. Adams and Victor's principles of neurology. McGraw Hill Medical,: New York, NY, 2014: 2v (xliii, 3,610, 158) .

74. Kubal WS. Updated imaging of traumatic brain injury. *Radiol Clin North Am.* 2012; 50(1): 15-41. doi: 10.1016/j.rcl.2011.08.010

75. Huisman TA. Diffusion-weighted and diffusion tensor imaging of the brain, made easy. *Cancer Imaging.* 2010; 10(1A): S163-S171. doi: 10.1102/1470-7330.2010.9023

76. Lin WC, Hsu TW, Chen CL, et al. Connectivity of default-mode network is associated with cerebral edema in hepatic encephalopathy. *PLoS One.* 2012; 7(5): e36986. doi: 10.1371/journal.pone.0036986

77. Koch S, Rabinstein A, Falcone S, Forteza A. Diffusion-weighted imaging shows cytotoxic and vasogenic edema in eclampsia. *AJNR Am J Neuroradiol.* 2001; 22(6): 1068-1070. doi: 10.1161/01.STR.28.5.1082

78. Maegele M, Stuermer EK, Hoeffgen A, et al. Multimodal MR imaging of acute and subacute experimental traumatic brain injury: time course and correlation with cerebral energy metabolites. *Acta Radiol Short Rep.* 2015; 4(1): 2047981614555142. doi: 10.1177/2047981614555142

79. Suetomi Y, Kanchiku T, Nishijima S, et al. Application of diffusion tensor imaging for the diagnosis of segmental level of dysfunction in cervical spondylotic myelopathy. *Spinal Cord.* 2015. doi: 10.1038/sc.2015.192

80. Barakat N, Gorman MP, Benson L, Becerra L, Borsook D. Pain and spinal cord imaging measures in children with

ISSN 2473-0947 Open Journal http://dx.doi.org/10.17140/ROJ-1-101

demyelinating disease. *Neuroimage Clin.* 2015; 9: 338-347. doi: 10.1016/j.nicl.2015.08.019

81. Lindberg PG, Sanchez K, Ozcan F, et al. Correlation of force control with regional spinal DTI in patients with cervical spondylosis without signs of spinal cord injury on conventional MRI. *Eur Radiol.* 2015. doi: 10.1007/s00330-015-3876-z

82. Chang ST, Xu J, Trinkaus K, et al. Optic nerve diffusion tensor imaging parameters and their correlation with optic disc topography and disease severity in adult glaucoma patients and controls. *J Glaucoma.* 2014; 23(8): 513-520. doi: 10.1097/IJG.0b013e318294861d

83. Smith SA, Williams ZR, Ratchford JN, et al. Diffusion tensor imaging of the optic nerve in multiple sclerosis: association with retinal damage and visual disability. *AJNR Am J Neuroradiol.* 2011; 32(9): 1662-1668. doi: 10.3174/ajnr.A2574

RADIOLOGY

Openventio PUBLISHERS

ISSN 2473-0947 Open Journal http://dx.doi.org/10.17140/ROJ-1-102

Review

*Corresponding author
Anthony Todd Dotson, MSRT, RT(R), (CT)
Assistant Professor of Imaging Sciences
Department of Kinesiology, Health & Imaging Sciences
Morehead University
316 West 2nd St., 210G CHER Building
Morehead, Kentucky 40351, USA
Tel. 606-783-5175
E-mail: a.dotson@moreheadstate.edu

Volume 1 : Issue 1
Article Ref. #: 1000ROJ1102

Article History
Received: November 18th, 2015
Accepted: February 23rd, 2016
Published: February 23rd, 2016

Citation
Dotson AT. Interoperability In radiography data: the impossible dream. *Radiol Open J*. 2016; 1(1): 13-16. doi: 10.17140/ROJ-1-102

Interoperability In Radiography Data: The Impossible Dream

Anthony Todd Dotson, MSRT, RT(R), (CT)*

Department of Kinesiology, Health & Imaging Sciences, Morehead University, Morehead, Kentucky 40351, USA

ABSTRACT

Background: Technology in healthcare is changing at a very rapid pace. To ensure that technology is used efficiently to combat rising healthcare costs and new federal policies and laws, all technology must be able to communicate with each other. Therefore, interoperability must be obtained. Radiography is no exception considering all the different types of equipment manufactured routinely used today. Some barriers need to be overcome to achieve interoperability within radiography departments.
Purpose: To review the literature on the interoperability of healthcare data to determine the barriers that Radiography departments would have to overcome to improve interoperability of their healthcare data.
Methods: The methodology of this literature review follows the fundamental principles of a systematic search, conducted in separate stages, but is not a comprehensive systematic review, which was not reasonable due to resource constraints. The stages of the literature search included defining the search strategy, identifying the inclusion criteria, assessing the relevance and validity of the studies retrieved, and data extraction and synthesis.
Results: There were attempts to ensure interoperability, such as the use of the Nationwide Health Information Network (NwHIN), but roadblocks such as financial incentives for physicians and costs of implantation have hindered the adoption of the NwHIN. Other barriers that limit interoperability exist. These obstacles included inconsistency of the Digital Imaging and Communication in Medicine (DICOM) standard for medical imaging departments and a complete lack of norms for certain data points such as the exposure index between different vendors.
Discussion: Multiple viable options for the improvement of interoperability are prevalent in radiography departments. One such option is cloud computing, which uses multiple various types of hardware and software as resources to help interoperability of healthcare data. Agent-based technologies, which can be used to distribute management of different standards, can also be utilized to communicate between standards. The largest need to ensure interoperability is standards that are well defined and stringent with an infrastructure to map different terminologies across different standards.
Conclusion: Various technological advances can be used to improve interoperability such as agent-based technology and cloud computing. However, until a standardization of terms within the DICOM protocol and a standard across vendors, and all data points standardized, it will be impossible to obtain true interoperability.

BACKGROUND

The technology used to communicate information in a healthcare setting is evolving at a rapid pace. In a typical radiology department, there are many different types of equipment. The same company does not manufacture equipment. To ensure that equipment can effectively communicate information to each other, interoperability must be obtained. Interoperability is the ability of one machine to identify and understand the information from another machine. In a typical radiology department, there is a variety of different software utilized to gather healthcare data. These include Electronic Health Records (EHR), Hospital Informa-

ISSN 2473-0947 Open Journal http://dx.doi.org/10.17140/ROJ-1-102

tion Systems (HIS), Radiology Information Systems (RIS), and Picture Archiving and Communication Systems (PACS).[1] Different types of software need to communicate to ensure that no information is lost. If they do not communicate, the institution would have to invest in an interface which will cost money, time, and manpower. An interface is a software that is created to convert data from one system to a format that another system can understand. If interoperability is achieved, the investment in an interface is unnecessary. Savings in costs are critical to the field of healthcare, where expenses have increased in recent years. At the end of the second quarter of 2014, the healthcare spending for the federal government increased at 4 percent annual rate.[2] Currently, the cost of health care has ballooned to an astounding $1.9 trillion.[3] With the total healthcare costs for the United States (U.S.) rising, constitutional laws now mandate health care providers use technology in meaningful ways. It is important for technology to benefit radiology departments by lowering costs and improving the efficiency of workflows. The significance of the research will be exploring and describing barriers to interoperability to help medical imaging departments reduce costs and timeliness of care.

President Obama has stated that the adoption of healthcare Information Technology (IT) will reduce errors, cut costs, ensure privacy and save lives.[4] Interoperability of the healthcare data is the only way any of the results listed by the president will happen. The goal of interoperability is sharing of healthcare information not only within any radiography department but across the continuum of care. One attempt to ensure interoperability across this continuum of care is the Nationwide Health Information Network (NwHIN). According to www.healthit.gov, the NwHIN website, the network is "a set of standards, services, and policies that enable the secure exchange of health information over the Internet."[5] NwHIN is a pathway to transmit data from one computer system to another. There are barriers to the adoption of the NwHIN. One such barrier is the cost of the implementation of the network. Estimations say that it would take one hundred and fifty-six billion dollars in capital costs to launch the NwHIN system. The largest issue to limit adoption of the NwHIN, however, is the lack of financial incentives for providers and institutions and the lack of national standards for data transmission.[6]

There have been many laws that addressed healthcare, and in turn, interoperability. The most recent law that influenced interoperability of healthcare data was the Affordable Care Act of 2010. This law instituted what was termed "meaningful use" of healthcare IT. Meaningful use is a program in Center for Medicare and Medicaid that gives guidelines to incentivize providers and organizations to use certified electronic health care records to improve care. There are three stages involved. The first phase started in 2011 and involved promoting adoption of EHR. The second stage focused on the coordination of care and exchanging patient data. The last step, to be rolled out in 2016, involves a focus on improving quality, safety, and efficiency of healthcare IT.[7] It would be impossible for this to happen without interoperability of different systems in the healthcare setting.

PURPOSE

The history of the political situation on healthcare IT resulted in the researcher's question of interoperability and the primary barrier that is present in radiography departments. The purpose of this exploratory research was to determine the primary barrier and identify possible solutions to support interoperability among different vendors and other systems used within a healthcare facility.

METHODOLOGY

The methodology of the literature review follows the fundamental principles of a systematic search, conducted in separate stages, but is not a comprehensive systematic review, which was not reasonable due to resource constraints. This limitation resulted in the inability to search 'gray literature' or to translate papers of a language other than English. However, the search did identify published major articles. The stages of the literature search included defining the search strategy, identifying the inclusion criteria, assessing the relevance and validity of the studies retrieved, along with data extraction and synthesis.

The literature review was limited to material from the last ten years to ensure the reliability of the information. Professional peer-reviewed journals, books, and professional websites regarding data transmission, healthcare IT management, or data standards were used during the research to ensure validity. The literature produced information that was then used to analyze data standards and to identify possible solutions to the lack of interoperability in radiography departments.

RESULTS

To realize the goal of achieving interoperability, first it must be possible to exchange healthcare data across different systems. Research completed in 2010 explains that there is a lack of interoperability partially because there are not structured data definitions or enough standards in the US.[8] Radiography departments utilize data from all across their organization from many different types of systems. The healthcare data used for radiological exams is the Digital Imaging and Communication in Medicine (DICOM) standard protocol. Radiography departments use DICOM protocols for viewing and diagnosing by the means of a PACS systems.[9]

DICOM data must be interpreted by other standard formats used in other software systems across the organization. One example is the Health Level 7 (HL7) standard utilized in the most electronic medical record (EMR) systems. The DICOM standard must also recognize data from many different types of vendors supplying equipment to the radiology department. This machine may use various types of data to determine the same

ISSN 2473-0947 Open Journal http://dx.doi.org/10.17140/ROJ-1-102

data point.

Although DICOM is the common standard for all imaging departments, the structure of the DICOM standard can vary between vendors. Sets of data are created in formats that are unique to the particular vendor that manufactures the equipment, which leads to some interoperability between imaging devices and PACS systems.[10] One example of this is the exposure index, where value is given to the dose received by a patient. Exposure index is an example of value that is present in all digital equipment, but a lack of standardization of the values between vendors limits the interoperability between different pieces of equipment. Different vendors use different values, and even some of the vendors that use the same values use different principles to calculate the data point.[11] Various data values make interoperability impossible for exposure index.

DISCUSSION

Data must be standard between systems to obtain interoperability. This standard requires constant data values.[12] The largest barrier to this is the lack or inconsistency of data standards used in today's radiography departments. There are many possible solutions to overcome this obstacle. One technology that is accustomed to some extent already that may change interoperability in the healthcare field is cloud computing. Cloud computing is services over the World Wide Web (WWW) where the multiple different types of hardware and software are facilitated in data centers to give the illusion of infinite resources so that data standards can communicate.[13] The use of these multiple data standards can be utilized on multiple data sets to improve interoperability.

Another solution could be in the form of agent-based technology. This type of technology has been proven to increase interoperability by distributing the management of sources of data, allowing remote access to patient data, and adapting font changes within the actual data standard.[14]

The largest need to ensure interoperability is a set infrastructure utilized by all that includes detailed mapping of different standards that can translate and code the terminologies of the various standards to ensure interoperability. This support should also contain input from professional societies, legal framework for accountability, and a way to translate, map, and transcode all of the terminologies involved.[15]

There are limitations evident during this research. One limitation of the study is the lack of common definitions associated with data standard criteria within the U.S. This lack of common definitions limited the resources available to access in regards to criteria for data standards. A second limitation of the research was that there was little available content found concerned the planning and design of technology systems in a digital health-care facility.[16]

CONCLUSION

Interoperability is considerably better among radiography departments than in most other technology fields. The interoperability is better because there are standards that widely accepted. Examples of these rules are DICOM and HL7. Full interoperability is still impossible because of variations in the DICOM standard are still present. A complete lack of standardization involving certain data points among vendor's equipment also presents a barrier to interoperability.

Some solutions will improve interoperability, such as agent-based technology and cloud computing. However, until a clear and standard terminology within DICOM is developed full interoperability will never be achieved. There also must be an avenue for accountability for not complying with this standard language. Cross-mapping of different terminologies of various standards and an infrastructure that supports and enforces that standardization is the only avenue to achieving true interoperability.

REFERENCES

1. Huang HK. *PACS and Imaging Informatics*. Hoboken, NJ, USA: John Wiley & Sons Publishing; 2010.

2. Furman J. Third Estimate of GDP for the Second Quarter of 2014. Web site. https://www.whitehouse.gov/blog/2014/09/26/third-estimate-gdp-second-quarter-2014 Published. September 26, 2014. Accessed September 2, 2015.

3. Sidorov J. It Ain't So: The Electronic Health Record and The Unlikely Prospect of Reducing Health Care Costs. *Health Aff (Millwood)*. 2006; 25(4): 1079-1085. doi: 10.1377/hlthaff.25.4.1079

4. Box T, McDonell M, Helfrich C, Jesse R, Fihn SD, Rumsfeld JS. Strategies from a Nationwide Health Information Technology Implementation: The VA Cart Story. *J Gen Intern Med*. 2010; 25 Suppl 1: 72-76. doi: 10.1007/s11606-009-1130-6

5. HealthIT.gov. Interoperability Portfolio (Archive). Nationwide Health Information Network (NwHIN). Web site. http://www.healthit.gov/policy-researchers-implementers/nationwide-health-information-network-nwhin. Updated. January 18, 2013. Accessed. August 12, 2015.

6. Kaushal R, Blumenthal D, Poon E, et al. of Cost of National Health Information Network Working Group. The costs of a national health information network. *Ann Intern Med*. 2005; 143(3): 165-173. doi: 10.7326/0003-4819-143-3-200508020-00002

7. Smith JB. What is Meaningful Use? *AONE*. 2013; doi: 10.1016/j.mnl.2013.01.006

ISSN 2473-0947 Open Journal http://dx.doi.org/10.17140/ROJ-1-102

8. Kumar S, Aldrich K. Overcoming barriers to electronic medical record (EMR) implementation in the US healthcare system: A comparative study. *Health Informatics J*. 2010; 16(4): 306-318. doi: 10.1177/1460458210380523

9. Koutelakis GV, Anastassopoulos GK, Lymberopoulos DK. Application of Multiprotocol Medical Imaging Communications and an Extended DICOM WADO Service in a Teleradiology Architecture. *International Journal of Telemedicine and Applications*. 2012; 271758: 1-11. doi: 10.1155/2012/271758

10. Crane JC, Olson MP, Nelson SJ. SIVIC: Open-Source, Standards-Based Software for DICOM MR Spectroscopy Workflows. *International Journal of Biomedical Imaging*. 2013; 169526: 1-12. doi: 10.1155/2013/169526

11. Källman H-E, Halsius E, Folkesson M, Larsson Y, Stenström M, Båth M. Automated detection of changes in patient exposure in digital projection radiography using exposure index from DICOM header metadata. *Acta Oncol*. 2011; 50(6): 960-965. doi: 10.3109/0284186X.2011.579622

12. Shea CM, Reiter KL, Weaver MA, et al. Stage 1 of the meaningful use incentive program for electronic health records: a study of readiness for change in ambulatory practice settings in one integrated delivery system. *BMC Med Inform Decis Mak*. 2014; 14: 119 doi: 10.1186/s12911-014-0119-1

13. Chen Y, Paxson V, Katz R. What's New about cloud computing security? EECS Department. University of California at Berkeley. Technical Report. 2010.

14. Urovi V, Olivieri AC, de la Torre AB, Bromuri S, Fornara N, Schumacher M. Secure P2P Cross-Community Health Record Exchange in IHE Compatible Systems. *Int J Artif Intell Tools*. 2014; 23: 1440006 doi: 10.1142/S0218213014400065

15. Chronaki C, Estelrich A, Cangioli G, et al. Interoperability standards enabling cross-border patient summary exchange. *Stud Health Technol Inform*. 2014; 205: 256-260. doi: 10.3233/978-1-61499-432-9-256

16. Beaty DL. Part One. Digital Healthcare Planning. *ASHRAE J*. 2014; 56(9): 84-90.

RADIOLOGY

Openventio PUBLISHERS

ISSN 2473-0947 Open Journal http://dx.doi.org/10.17140/ROJ-1-103

Case Report

*Corresponding author
Yuko Kobashi, MD
Department of Radiology
Tokyo Dental College
Ichikawa General Hospital
5-11-13 Sugano, Ichikawa
Chiba 272-8513, Japan
Tel. +81-47-322-0151
Fax: +81-47-325-4456
E-mail: ykobashi@jikei.ac.jp

Volume 1 : Issue 1
Article Ref. #: 1000ROJ1103

Article History
Received: February 9th, 2016
Accepted: March 10th, 2016
Published: March 14th, 2016

Citation
Kobashi Y, Ogiwara S, Fukuda K, Kubota M. Tarsal tunnel syndrome due to varicose vascular structures: a case report. *Radiol Open J*. 2016; 1(1): 17-20. doi: 10.17140/ROJ-1-103

Tarsal Tunnel Syndrome Due To Varicose Vascular Structures: A Case Report

Yuko Kobashi, MD[1*]; Shou Ogiwara, MD[2]; Kunihiko Fukuda, MD[2]; Makoto Kubota, MD[3]

[1]Department of Radiology, Tokyo Dental College Ichikawa General Hospital, 5-11-13 Sugano, Ichikawa, Chiba 272-8513, Japan
[2]Department of Radiology, Tokyo Jikei University School of Medicine, Nishi-Shimbashi, Minato-ku, Tokyo 105-8461, Japan
[3]Department of Orthopedics, Tokyo Jikei University School of Medicine, Katsushika Medical Center, 6-41-2, Aoto, Katsushikaku, Tokyo, 125-8506, Japan

ABSTRACT

Objective: We report a case of a tarsal tunnel syndrome caused by a varicose vascular structures identified by foot MRI.
Case report: An eighty-year old male came to our attention for a chronic intermittent bilateral plantar numbness. Symptoms were evident especially in the left foot when taking a bath or after a long distance walk. Feet were bilaterally flat. Ankles range of motion was bilaterally complete and pain free. Resisted range of motion testing including resisted ankle dorsiflexion, plantar flexion, inversion, and eversion was found to be pain free and of equal strength bilaterally**.** Neurological testing of the lower extremities was found to be positive for the Tinel sign at level of medial malleolus. Left ankle MRI showed evidence of several varicose vascular structures. One of the varicose vascular structures was suddenly narrow at level of tarsal tunnel. Posterior tibial vein at the tarsal tunnel level was dilated and appeared to continue in the varicose vascular structure on contrast study. Diagnosis of tarsal tunnel syndrome was made both by symptoms and imaging, considering the dilatation of the posterior tibial vein and the compression of the varicose structures around the tarsal tunnel.
Treatment: Resection surgery of the retinaculum was performed in order to decrease the pressure on the tarsal tunnel. The patient's symptom reduced after the surgery. However, a few months later he referred recurrence of plantar numbness.
Conclusion: Patients who suffer from tarsal tunnel syndrome caused by a varicose vascular structures can show different symptoms if compared with those present in the same syndrome caused by other diseases. If varicose veins are detected in the tarsal tunnel and symptoms of compression are present, along with a concomitant foot deformity that predisposes to disease, diagnosis of tarsal tunnel syndrome should be considered. In order to achieve good results, the treatment of the varicose vascular structures and the correction of foot deformities are recommended together with a tarsal tunnel decompression.

KEYWORDS: Tarsal tunnel; Varicose vascular structure; MRI.

INTRODUCTION

The tarsal tunnel is a fibro-osseous space found in the medial aspect of the ankle, posterior to the medial malleolus, bounded by the flexor retinaculum superiorly, and by the medial walls of the distal tibia, talus and calcaneus inferiorly. The tendons of tibialis posterior, flexor digitorum longus and flexor hallucis longus, the posterior tibial nerve, artery and vein run together through the tarsal tunnel.[1,2] The tarsal tunnel syndrome can be caused by extrinsic or intrinsic pressure on the posterior tibial nerve or on its terminal branches: the medial plantar nerve, the lateral plantar nerve, the medial calcaneal nerve, the motor branch to the abductor muscle of the fifth toe and/or the inferior calcaneal nerve.[1,2] Diagnosis is usually based on physical examination and can be confirmed by electrophysiological evidence. The treatment of the tarsal tunnel syndrome varies depending on the cause that underlies the pathology.

ISSN 2473-0947 Open Journal http://dx.doi.org/10.17140/ROJ-1-103

We report a case of a tarsal tunnel syndrome caused by a varicose vascular structures identified by foot MRI.

CASE REPORT

An eighty-year old male came to our attention for a chronic intermittent bilateral plantar numbness affecting him from 5 years. Symptoms were evident especially in the left foot when taking a bath or after a long distance walk. The plantar numbness was not caused by his shoes. On physical examination, the patient showed no muscular atrophy. Flat foot deformity was present bilaterally and a lot of varicose vascular structures in both lower extremities were observed. The patient referred paresthesias and lack of sensation in both lower legs and in foot dorsal and plantar areas. The ranges of motion testing of the cervical and lumbar spines were found to be full and pain free in all directions**.** The range of motion of the ankles was full and pain free bilaterally. Resisted range of motion testing including resisted dorsiflexion, plantar flexion, inversion, and eversion of the ankle was found to be pain free and of equal strength bilaterally**.** Neurological testing of the lower extremities was found to be positive for the Tinel sign at the medial malleolus level. Non weight bearing examination of the feet uncovered 'medium' and approximately equal plantar longitudinal arch height bilaterally. Toe and heel walking were unremarkable bilaterally. No Hallux deformity was detected. Bilateral weight bearing feet x-rays showed evidence of soft tissue swelling around ankles, suggesting the presence of varicose vascular structures. There was no evidence of bony fusion or other bones deformity in both ankles and feet. Left ankle MRI showed evidence of a lot of varicose vascular structures mainly medical aspect in the lower part of the leg and foot on T1 weighted axial (TR/TE 518/20 ms, Thickness 3 mm, gap 03. mm and FOV 160 mm) and T2* weighted sagittal image (TR/TE 430/14 ms, Thickness 3 mm, gap 03. mm and FOV 160 mm) (Figure 1a and b). One of the varicose vascular structures was suddenly narrow at level of tarsal tunnel. In addition, posterior tibial vein at the tarsal tunnel was dilated on gadolinium enhanced fat suppression T1 weighted axial image (TR/TE 518/20 ms, Thickness 3 mm, gap 03. mm and FOV 160 mm) (Figure 2a) and appeared to continue with the varicose vascular structure (Figure 2b). Deep venous system thrombosis of the left lower leg was uncertain on this MRI. These findings suggested that superficial venous valve insufficiency caused a blood regurgitation and dilatation not only in superficial veins but also in posterior tibial vein and through some communicating branches between superficial vein and posterior tibial vein. The right MRI was not taken at first time. From both the physical examination and the left MRI findings, we diagnosed a tarsal tunnel syndrome caused by a dilatation of the posterior tibial vein and by a compression of the varicose structures around the tarsal tunnel.

On surgical findings, the dilated posterior tibial vein got tighter under the retinaculum of tarsal tunnel (Figure 3a). Varices formations continued into the posterior tibial vein and were present at both superior and inferior aspect of the retinaculum. A surgical resection of the retinaculum was performed in order to decrease the pressure on the tarsal tunnel (Figure 3b). The patient's symptoms reduced after surgery. However a few months later, he referred plantar numbness again.

DISCUSSION

Various conditions have been suggested to play a role in the etiology and pathogenesis of a posteromedial tarsal tunnel syndrome. This syndrome can be idiopathic (in about 50% of cases) or associated with space occupying lesions including tumors, ganglion cysts from the subtalar joint or tendon sheaths, abnormal or accessory muscle (hypertrophic adductor hallucisor accessory flexor digitorum longus muscle,[3,4] lipomas, varicose veins, trauma with bone spicule from an adjacent fracture, foreign bodies, iatrogenic causes such as calcaneal osteotomies with involuntary deep penetration medially, with fixation hardware or scar tissue.[3,5]

Tarsal tunnel syndrome may also develop in relation

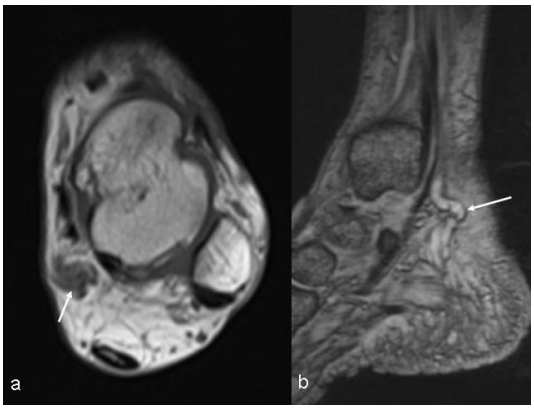

Figure1: Varicose vascular structure at level of tarsal tunnel.
a. T1 weighted axial image (TR/TE 518/20 ms, Thickness 3 mm, gap 03. mm and FOV 160 mm) shows evidence of dilated vessel suggestive of varix at level of the right tarsal tunnel (arrow).
b. T2* weighted sagittal image (TR/TE 430/14 ms, Thickness 3 mm, gap 03. mm and FOV 160 mm)shows dilated superficial vein at posterior aspect of medial malleolus (arrow).

ISSN 2473-0947 Open Journal http://dx.doi.org/10.17140/ROJ-1-103

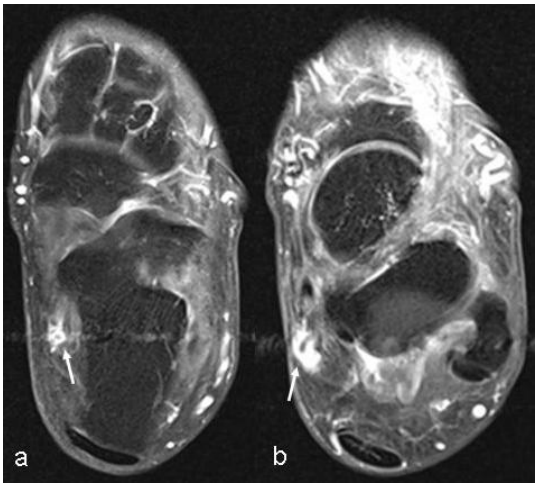

Figure2: The varix and dilated posterior tibial vein at level of tarsal tunnel.

a. Posterior tibial vein (arrow) is dilated and is strongly enhanced on gadolinium enhanced fat suppression T1 weighted axial image (TR/TE 518/20 ms, Thickness 3 mm, gap 03. mm and FOV 160 mm).

b. A varix is present just above of the tarsal tunnel (arrow). This varicose vascular structure is continued to posterior tibial vein on gadolinium enhanced fat suppression T1 weighted axial image.

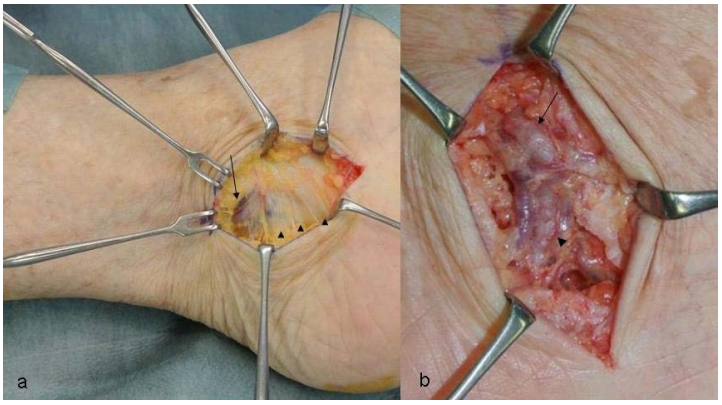

Figure3: Surgical findings of tarsal tunnel.

a. The varix (arrow) just above the tarsal tunnel is demonstrated. Thin superior retinaculum (arrowheads) is visualized.

b. Resection of the superior retinaculum was performed. The varix (arrow) is continued to the posterior tibial vein (arrowhead) under the superior retinaculum through communicating vein. These findings may suggest regurgitation of venous vessels from superficial vein to posterior tibial vein.

to some foot deformities such as valgus /varus deformity, pes planus and tarsal coalition. Systemic diseases such as diabetes, rheumatoid arthritis and peripheral arterial disease can play a role in this syndrome. The main symptoms of tarsal tunnel syndrome are represented by poorly localized paresthesia, dysesthesia and hypoesthesia in the medial and lateral plantar area**.** Symptoms are typically unilateral and rarely bilateral.[6] Tarsal tunnel syndrome caused by varicosity may show characteristic symptoms: Kumai et al[7] reported that patients suddenly feel foot pain whenever they soak a foot in hot water. This specific symptom occurs due to dilatation of the varicose vascular structures in the tarsal tunnel. Our patient had the same symptom thus supporting the hypothesis that the tarsal tunnel syndrome was caused by the varicose vascular structures compression.

Sato et al[8] reported a frequency of tarsal tunnel syndromes caused by the varicose vascular structures of about 4% and in the literature they represent about 14% of the cases described.[9] On the other hand, 43% of Japanese people (48 million people) over 15 years or older, have varicose vascular structures.[10,11] Although there are many patients who have had widespread varicose veins, they are rarely complicated with a tarsal tunnel syndrome. It would be because the varicose vascular structures cannot cause a tarsal tunnel syndrome alone if they are not at the tunnel level**.** Varicose veins are also associated to flat foot and heel valgus: this condition creates a compression of the plantar nerves and can cause a tarsal tunnel syndrome as well**.** In addition, tarsal tunnel syndrome symptoms might be masked by other symptoms caused by the varicose vascular structures like legs and feet swelling, feet early fatigue, skin alterations and venous ulcers.[12,13] We were able to diagnose the tarsal tunnel syndrome, but we should have treated the varicose vascular structures after the surgical resection of the retinaculum, in order to avoid a relapse of the tarsal tunnel syndrome as reported in the literature.[13,14] Moreover, even the flatfoot deformity, which can play a role in the pathogenesis of the syndrome, should have

ISSN 2473-0947 Open Journal http://dx.doi.org/10.17140/ROJ-1-103

been considered in the treatment strategy as well.

We first chose MRI to evaluate the tarsal tunnel syndrome because we initially suspected a space occupying lesions like ganglion cysts, but in this case we should have taken a contrast enhanced CT for the varicose vascular structures.

CONCLUSION

Tarsal tunnel syndrome can be caused by varicose vascular structures and patients who suffer from this syndrome may show characteristic symptoms. If varicose veins are in the tarsal tunnel and if a foot deformity is present a diagnosis of tarsal tunnel syndrome due to varicose vascular structures compression should be considered. In order to make a proper diagnosis, it is mandatory to evaluate the status of the varicose vascular structures at first. Treatment of the varicose vascular structures and correction of eventual foot deformity are recommended in association with a tarsal tunnel decompression.

CONSENT

The patient has provided written permission for publication of the case details.

CONFLICTS OF INTEREST

The authors declare that they have no conflicts of interest.

REFERENCES

1. Baghla DPS, Shariff S, Dega R. Calcaneal osteomyelitis presenting with acute tarsal tunnel syndrome: a case report. *J Med Case Reports*. 2010; 4: 66. doi: 10.1186/1752-1947-4-66

2. Antoniadis G, Scheglmann K. Posterior Tarsal Tunnel Syndrome: Diagnosis and Treatment. *Dtsch Arztebl Int*. 2008; 105(45): 776-781. doi: 10.3238/arztebl.2008.0776

3. Erickson SJ, Quinn SF, Kneeland JB, et al. MR imaging of the tarsal tunnel and related spaces: normal and abnormal findings with anatomic correlation. *AJR Am J Roentgenol*. 1990; 155(2): 323-328. doi: 10.2214/ajr.155.2.2115260

4. Ormeci T, Mahirogulları M, Aysal F. Tarsal tunnel syndrome masked by painful diabetic polyneuropathy. *Int J Surg Case Rep*. 2015; 15: 103-106. doi: 10.1016/j.ijscr.2015.08.033

5. Gould JS. Tarsal tunnel syndrome. *Foot Ankle Clin*. 2011; 16(2): 275-286. doi: 10.1016/j.fcl.2011.01.008

6. Abouelela AA, Zohiery AK. The triple compression stress test for diagnosis of tarsal tunnel syndrome. *Foot (Edinb)*. 2012; 22(3): 146-149. doi: 10.1016/j.foot.2012.02.002

7. Kumai T, Takakura Y, Kitada C. *Tarsal tunnel syndrome: The foot-clinical instruction with illustration* [In Japanese]. 3rd ed rev. 2010: 184-187.

8. Satoh K, Kanazawo N, Egawa M. Clinical study on tarsal tunnel syndrome [In Japanese]. *Seikei-Geka*. 1986; 37: 271-279.

9. Cimino WR. Tarsal tunnel syndrome: review of the literature. *Foot Ankle*. 1990; 11(1): 47-52.

10. Sammarco GJ, Conti SF. Tarsal tunnel syndrome caused by an anomalous muscle. *J Bone Joint Surg Am*. 1994; 76: 1308-1314.

11. Hirai T, Kubota H, Kawamura Y, et al. Prevalence and risk factors of primary varicose veins [In Japanese]. *Japanese College of Angiology*. 1988; 28: 415-420.

12. Joh JH, Kim WS, Jung IM, Park KH, Lee T, Kang JM; Consensus Working Group. Consensus for the Treatment of Varicose Vein with Radiofrequency Ablation. *Vasc Specialist Int*. 2014; 30(4): 105-112. doi: 10.5758/vsi.2014.30.4.105

13. Gould N, Alvarez R. Bilateral tarsal tunnel syndrome caused by varicosities. *Foot Ankle*. 1983; 3(5): 290-292. doi: 10.1177/107110078300300510

14. Ahmad M, Tsang K, Mackenney PJ, Adedapo AO. Tarsal tunnel syndrome: A literature review. *Foot Ankle Surg*. 2012; 18(3): 149-152. doi: 10.1016/j.fas.2011.10.007

RADIOLOGY

Openventio PUBLISHERS

ISSN 2473-0947 Open Journal http://dx.doi.org/10.17140/ROJ-1-104

Research

*Corresponding author
Andreas A. Linninger, PhD
Department of Bioengineering and Neurosurgery, University of Illinois
851 S. Morgan St
218 SEO, M/C 063
Chicago, IL, USA
Tel. 708-214-2264
Fax: 312-413-7803
E-mail: linninge@uic.edu

Volume 1 : Issue 1
Article Ref. #: 1000ROJ1104

Article History
Received: April 15th, 2016
Accepted: May 13th, 2016
Published: May 18th, 2016

Citation
Hsu CY, Alaraj A, Linninger AA. Cerebral blood flow assessment by digital subtraction angiography. *Radiol Open J*. 2016; 1(1): 21-30. doi: 10.17140/ROJ-1-104

Cerebral Blood Flow Assessment by Digital Subtraction Angiography

Chih-Yang Hsu, BS[1]; Ali Alaraj, MD[2]; Andreas A. Linninger, PhD[3*]

[1]Department of Bioengineering, University of Illinois, Chicago, IL, USA
[2]Department of Neurosurgery, University of Illinois, Chicago, IL, USA
[3]Department of Bioengineering and Neurosurgery, University of Illinois, Chicago, IL, USA

ABSTRACT

Cerebral vascular disease is responsible for nearly 800 000 hospital admissions annually with a total healthcare cost of $34 billion. Neuro-interventional surgery is at the forefront of fast-response assessment and intervention to assess patients' health using digital subtraction angiography (DSA). Unfortunately, cerebral blood flow cannot be reliably measured with DSA during intervention. In this study, we introduced a novel inversion-based method to quantify blood flow from DSA intensity profiles. This technique yields absolute volumetric flow rates in major cerebral arteries comparable in accuracy to QMRA measurements. This remarkable outcome was achieved by incorporating patient-specific anatomical data as well as flow physics into the image analysis. The inversion-based flow assessment is a promising approach to render absolute flow measurements with traditional DSA. We also discuss the precision of several methods for assessing cerebral blood flow before and after intervention in DSA were investigated. Angiographic intensity data in four patients with cerebral vascular diseases were analyzed to compute time-to-peak index (TTPi) and relative cerebral angiographic blood flow index (RCABi). Flow indices were compared with quantitative magnetic resonance angiography acquired pre- and post-intervention. The results suggest that individual intensity-based flow indices do not always reflect blood flow improvements after intervention; two-dimensional index maps showed the improvements more robustly.

KEYWORDS: Image processing; Intracranial blood flow; Inversed blood flow.

INTRODUCTION

Digital subtraction angiography (DSA) is the preferred technique in immediate assessment of blood flow for patients with cerebral vascular diseases during neurovascular intervention.[1-5] However, assessment of vascular status in a given patient currently depends on the physicians' intuitive judgment of dynamic contrast agent distribution patterns observed with DSA. Current DSA technology does not display volumetric blood flow rates. Flow in major cerebral blood vessels can be measured with other non-invasive imaging modalities including quantitative magnetic resonance angiography (QMRA),[6,7] Xenon-enhanced cerebral tomography,[8] single-photon emission computed tomography,[9,10] or transcranial Doppler sonography.[11] Moreover, perfusion studies in computed tomography, magnetic resonance imaging and positron emission tomography[12] enable clinical measurements of microcirculation. However, these advanced imaging modalities are not available during surgery due to space requirements of the scanners. Some procedures are further limited by acceptable radiation dosage and unavailability of these techniques in smaller hospitals. Some studies[13-15] have also cast doubt on perfusion methods for identifying infarct regions, because they involve image interpretation with respect to arbitrary mismatch thresholds.

Recently, increased acquisition rate in combination with de convolution analysis are beginning to provide metrics of cerebral blood flow, cerebral blood volume and mean transit time using DSA with dual panel detectors.[16-18] Especially, absolute blood flow quantification

ISSN 2473-0947 Open Journal http://dx.doi.org/10.17140/ROJ-1-104

in large vessels would be significant to improve the diagnostic capability of DSA. Precise blood flow metrics would help the neuro-interventionalist in defining end Points for the intervention. Blood flow metrics in addition to contrast agent distribution patterns would also ease physicians' decision making during interventional procedures.

Accordingly, there is considerable research interest in quantifying blood flow with conventional DSA. Waechter[19,20] used model-based waveform analysis of the pixel intensity. Tenjin[21] correlated mean transit time and peak time to blood flow. Kamp[22] performed indo-cyanine green fluorescence angiography during surgery to correlate intensity-time plots to relative blood flow on exposed cortical surfaces. Lieber[23] performed micro droplet angiography during selective catheterization to access flow within arteriovenous malformations. Other analytical methods interpret slopes and extremes of the intensity profiles for flow analysis.[24-26] Inversion-based methods use parameter estimation to infer volumetric blood flow rates.[27-29] In an extensive review on blood flow estimation,[30] *inversion* was assessed as the most rigorous technique, but also deemed computationally extensive.

In this paper, we first evaluate the consistency and precision of two intensity-based metrics: (i) the *relative cerebral angiographic blood flow index* (RCABi) and (ii) the *time-to-peak index* (TTPi). We use four clinical symptomatic arterial steno-occlusive disease cases studies to examine the benefits and limitations of simple flow metrics at baseline and post angioplasty and stenting. We compare flow estimates to volumetric flow rates acquired *in vivo* for all patients with baseline and post intervention QMRA. We further propose a new inversion technique for blood flow quantification with conventional DSA. The novel technique determines the volumetric flow rates in major arteries by perfectly aligning the DSA concentration profiles measured *in vivo* with computer predictions performed on a patient-specific blood flow network. We show that DSA absolute blood flow measurements almost reach QMRA accuracy.

MATERIALS AND METHODS

A. DSA acquisition of four patients pre and post intervention

Four patients with steno-occlusive disease were studied. All patients had symptomatic intracranial stenosis that requires angioplasty and stenting intervention. Standard diagnostic DSA data were acquired for all four patients 1-4, before and after intervention from the practice of the Endovascular Section - Department of Neurosurgery at our institution in accordance with Institutional Review Board approved protocols. Age, gender, disease diagnosis, and blood flow assessment of these patient cases can be found in Table 1. All patients had baseline and post-intervention angiograms. Contrast agent was injected into the patients' internal carotid artery (ICA) in patients 2-4, and into the venous graft supplying the ICA territory for patient-1. In all four cases, there was evidence of diminished intracranial flow in the middle cerebral artery (MCA) as documented by QMRA. DSA data with three frames per second were collected before and after intervention (Leonardo, Siemens; Malvern PA). Dynamic contrast agent distribution was acquired by performing a typical bolus injection in the injected artery. The vasculature of the main arterial network was captured from images taken after constant infusion. DSA images were acquired and stored in DICOM format.

B. Intensity-based flow indices

DSA intensity plots were analyzed with regards to the change in time-to-peak and peak intensity. The relative cerebral angiographic blood flow index (RCABi) was defined as the ratio of the maximum intensity over the rise rate in selected vessels of interest. The rise rate was defined as the time needed for the intensity profile to reach maximum from 25% level of the maximum intensity. The time-to-peak index (TTPi) for a pixel inside an artery was defined as the time needed for the intensity to reach its maximum. We selected individual pixels in vessels of interest to calculate RCABi and TTPi. We also generated two-dimensional maps after computing the RCABi and TTPi for all pixels of the two DSA projection planes. The pixel-by-pixel analyses as well as the two-dimensional maps were generated for both the pre- and post-interventional angiography data.

C. Patient MRI acquisition

To set an independent gold standard for blood flow in major arterie, we acquired cervical and intracranial vessels quantitative MRA non-invasive optimal vessel analysis (QMRA NOVA, Vas Sol Inc. River Forest, IL) measurements before and after intervention. The details of obtaining a QMRA NOVA report are reported elsewhere.[6,7] NOVA reports were used as the gold standard and reference to validate flow indices. QMRA measurement was limited to the major branches of the Circle of Willis and proximal branches; small arteries are not accessible to NOVA due to limited MR image resolution.

D. Flow calculation from DSA by image inversion

We propose a novel method to estimate volumetric blood flow rates from DSA images. To uniquely determine blood flow by indirect observation of the contrast agent distribution in space and time, we solved a parameter estimation problem that minimizes the difference between DSA contrast agents intensity and contrast agent profiles simulated for the anatomical hemodynamic network of each patient. The inclusion of anatomical information and flow physics will be shown to be advantageous for accurate blood flow predictions. Parameter estimation, also known as *inversion*, constitutes a non-linear optimization problem with objective function given in (1) subject to partial differential equation constraints (2-4) The inversion requires three components: (i) intensity plots (ii) an anatomical vascular network model (iii) hemodynamics and an inversion algorithm.

ISSN 2473-0947 Open Journal http://dx.doi.org/10.17140/ROJ-1-104

$$\min_{P,F} \left\| \frac{\hat{C}(F,P,t) - C(t)}{C(t)} \right\|^2 \quad (1)$$

s.t.

$$\vec{\nabla} \cdot F = 0 \quad (2)$$

$$F = \frac{A}{\alpha}\Delta P \text{ where } \alpha = \frac{8\mu L}{\pi d^4} \quad (3)$$

$$V\frac{d\hat{C}}{dt} + \frac{F}{A}\vec{\nabla}C = 0 \quad (4)$$

(i) Intensity Plots: Several regions of interest were chosen corresponding to the major arteries connected to the Circle of Willis. Although the method has no such limitation, DSA infusions are often performed only on one side of the patient. In our cases, three patients were injected in the right hemisphere, only patient-1 was infused in the left hemisphere. The image intensities were obtained from the respective DSA frames with the chosen locations in the infused hemisphere. We selected areas of interest including pixels located inside the internal carotid arteries (ICA), middle cerebral arteries (MCA), anterior cerebral arteries (ACA), posterior cerebral arteries (PCA), posterior communicating arteries (PCOM), basilar artery (BA), and anterior communicating artery (ACOM) as shown in Figure 5A.

(ii) An anatomical vascular network model: To relate blood flow and contrast agent intensity distribution acquired with DSA, a computational model of blood flow and dynamic contrast agent convection was established using the patient-specific anatomical network of the cerebral vasculature. We generated a morphologically accurate computer model of the main cerebral arteries emerging from the patients' Circle of Willis. Due to the unilateral contrast injection used in clinical practice, our model captured only the injected hemisphere. 3D rotational angiography data obtained in patients were used for reconstructing a network model in which each blood vessel was represented by a cylindrical segment of known length and diameter. A stack of 508 DSA images with a resolution of 512×512 were segmented by manually chosen thresholds for reconstructing blood vessel surfaces with the marching cubes algorithm.[31] The center lines of segmented vessels and their diameters were delineated using vascular modeling toolkit.[32] Due to limited image resolution, only the main cerebral arteries (above a diameter of d>1 mm) could be reliably reconstructed. Accordingly, the major blood vessels of the right hemisphere of patient-2 and patient-4 were reconstructed.

(iii) Hemodynamics and inversion algorithm: We carefully incorporated patient-specific data such as diameters and segment length of the main arteries around the Circle of Willis into the blood flow network model. Hemodynamic computations were based on simple network flow models described previously by other authors, ignoring the effects of oscillatory wave propagation and reflection.[33,34] In brief, continuity was applied as shown in (2), where F is the blood flow. Pressure drop was approximated using Poiseuille's law given in (3), where d, A and L are the diameter, cross sectional area and length of a vascular segment, ΔP is pressure drop, μ is the apparent blood viscosity. This simple hemodynamic network model composed of cylindrical segments was also used to predict convection of a non-dilutable contrast agent as given in (4). The dynamic concentration profiles for contrast injected into the patient cerebral arteries were computed by the species conservation balance, where V is the volume of a small vascular segment, and C is its contrast agent concentration. Inversion with hemodynamic principles as side conditions was performed to compute the specific blood flows and pressures that best aligned the measured concentration profiles with predicted profiles. The objective function was minimized by adjusting the pressure boundary conditions at the internal carotid artery and peripheral arterial terminal vessels of interest to achieve the best match between the contrast concentration profiles. Specifically, concentration profiles were extracted from the RICA, RMCA, RACA, and LACA for patient-2. In patient-4, RICA, RMCA, and RACA concentration profiles were used in the inversion.

RESULTS

The results are presented according to the hierarchy displayed in Figure 1. We first present the intensity-based indices. These indices are compared with flow measurement from QMRA. Finally we show the results of the *novel inversion technique* to estimate absolute blood flow with conventional DSA.

DSA intensity-based flow indices

Patient-1 was treated initially for a giant right ophthalmic ICA segment aneurysm with ICA sacrifice and extracranial-intracranial venous graft bypass. The vein graft developed progressive stenosis, with compromise of left MCA flow. The arteries of interest were LMCA, LACA, and LACA2. All results are shown in Table 1. Before intervention, the time-to-peak indices were determined to be TTPi=2.94±0.61, 2.52±0.54, and 3.36±0.33, the relative cerebral blood flow indices were RCABi= 0.20±0.04, 0.15±0.04, and 0.12±0.03. Post angioplasty and stenting of the stenotic venous graft, the TTPi was determined to be 1.14±0.13, 1.15±0.14, and 1.50±0.01, the RCABi was 0.45±0.09, 0.35±0.04, and 0.32±0.06. Decrease in the TTPi and increase in the RCABi clearly indicate the improvement of blood flow. The relative change of TTPi in LMCA, LACA, and LACA2 were 61%, 55%, and 54%. The relative change of RCABi in LMCA, LACA, and LACA2 were 56%, 57%, and 63%. The absolute flow change in QMRA in LMCA and LACA were 40% and 35%. LACA2 measurement was not available in post-treatment QMRA. Table 1 summarized the intensity-based flow indices in various locations of interest for all four patients before and after intervention. In all four cases, the neurovascular intervention improved blood supply to the patients' compromised cerebral hemispheres. We further computed the statistical

ISSN 2473-0947 Open Journal http://dx.doi.org/10.17140/ROJ-1-104

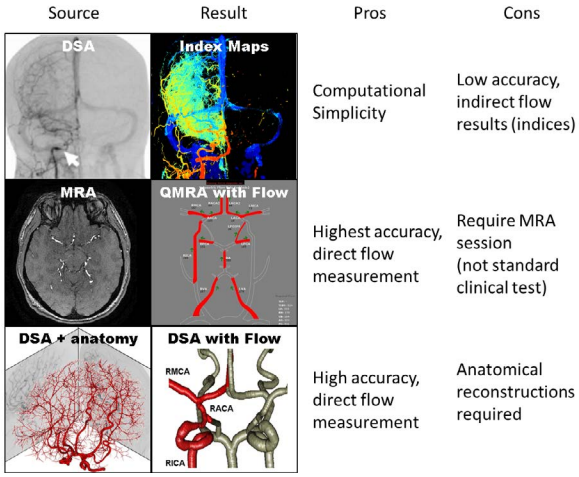

Figure 1: Schematic of various modes of blood flow assessment using different imaging modalities. (Top) Simple flow indices can be derived by DSA images but only shows relative changes. (Middle) Absolute volumetric blood flow rates can be acquired by performing quantitative MRA, which is not available in the interventional setting. (Bottom) The novel inversion technique presented in this paper integrates DSA intensity profiles with anatomical information to predict measure volumetric blood flow rates with reasonable speed and accuracy. Red vessels indicate the major vessels observed from DSA reconstruction in the infused hemisphere, gray vessels indicate the unobservable vessel in the contra-lateral hemisphere.

		Patient 1	Patient 2	Patient 3	Patient 4
Age		67	48	45	43
Gender		Female	Female	Male	Female
Diagnosis		Vein graft stenosis	RICA stenosis	RICA stenosis	RICA stenosis
QMRA (mL/min)	ICA(Pre/Post)	--/--	93/289	--/275	94/205
	MCA(Pre/Post)	-34/-57	58/157	57/215	58/175
	ACA(Pre/Post)	58/89	23/105	-12/133	14/49
	ACA2(Pre/Post)	44/--	35/68	43/104	20/47
TTPi (s)	ICA(Pre/Post)	--/--	2.58/1.50	1.80/0.72	1.02/0.66
	MCA(Pre/Post)	2.94/1.14	3.12/1.86	1.86/1.14	0.90/0.84
	ACA(Pre/Post)	2.52/1.14	3.18/1.74	2.25/1.98	1.23/0.96
	ACA2(Pre/Post)	3.36/1.50	2.94/1.68	1.65/1.50	0.98/0.78
RCABi (s)	ICA(Pre/Post)	--/--	0.24/0.36	0.57/0.80	0.34/0.84
	MCA(Pre/Post)	0.20/0.45	0.13/0.17	0.47/0.42	0.14/0.26
	ACA(Pre/Post)	0.15/0.35	0.14/0.20	0.43/0.47	0.37/0.33
	ACA2(Pre/Post)	0.12/0.32	0.15/0.46	0.41/0.39	0.18/0.14
Inversion (mL/min)	ICA(Post)	--	263.6±2.6*	--	182.9±6.1*
	MCA(Post)	--	168.5±4.0*	--	136.6±6.0*
	ACA(Post)	--	56.5±2.5*	--	50.1±6.2*

The QMRA NOVA flow measurement has the unit of mL/min, --stands for unavailable, - sign indicates reversed flow. * Stands for 99% confidence region.

Table 1: Patient case description.

agreement between blood flow and intensity-based indices as shown in Figure 2. For this purpose, we plotted on the x-axis the measured QMRA flow rate and on the y-axis the RCABi and the inverse of the TTPi at the same artery. Because flow measurements were available for four arteries, multiple data points were available for comparison. We also performed linear regression to correlate intensity-based indices against QMRA-based blood flow.

Rcabi And Ttpi For Intervention Assessment

The scatter plots in Figure 2 show trends, which seem to support the notion that higher RCABi are associated with higher blood flow as expected. However, a closer look at Figure 3B demonstrates individual pixels that disagree with the flow improvements. When plotting the blood flow changes before and after intervention trends with QMRA and RCABi, it can be

ISSN 2473-0947 Open Journal http://dx.doi.org/10.17140/ROJ-1-104

seen that an increase in blood flow detected by QMRA is not even qualitatively captured by the corresponding RCABi in the MCA. Accordingly, a local RCABi in the RACA erroneously suggests a blood flow decrease, when in fact it has increased. On the other hand, the trends of Figure 3B show no inconsistencies in the inferred blood flow changes with TTPi. The TTPi reflected correctly improved blood flow in all four cases. Flow indices shown in Figure 2 are in agreement with the general trend of flow improvement after surgical intervention. However, the lack of fit underscores the limitations of these simple indices as quantitative blood flow metrics. The low R^2-value in the scatter plots (RCABi: R^2=0.25, 0.19, 0.50, 0.68; TTPi: R^2=0.55, 0.56, 0.34, 0.11) reflects only a weak correlation between indices and absolute volumetric flow rates.

Two-dimensional TTPi and RCABi maps were also generated for coronal planes as shown in Figure 3A. Recently, similar maps are being offered as upgrades to existing angiography suite software. The two-dimensional plots show color patches reflecting the improved blood flow after interventions. In all

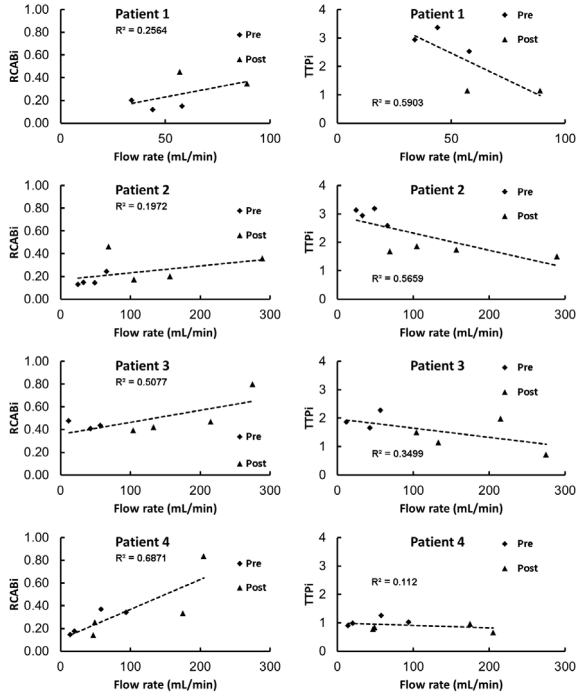

Figure 2. Scatter plot of inversion-based flow indices against QMRA flow measurement. Left: RCABi against flow shows overall increase of RCABi indicates faster flow rates. Right: TTPi against flow shows overall decrease of TTPi indicates faster flow rates. Multiple measurements for numerous blood vessels were available for each patient for better comparison.

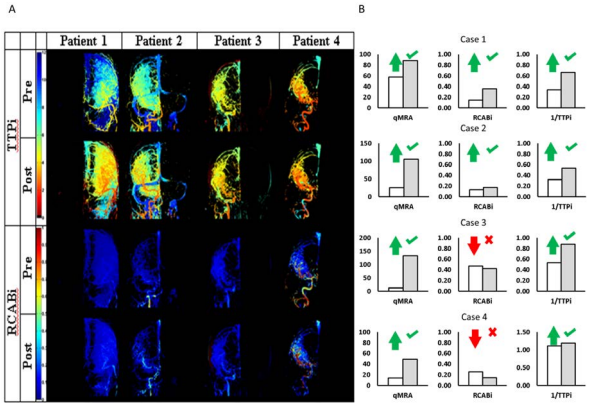

Figure 3: Pre- and post- treatment intensity-based flow indices. (A) Two-dimensional flow maps showing an overall decrease in TTPi and increase in RCABi suggesting an improvement of blood flow after intervention. The success of the treatment effect can be observed based on flow indices derived from the dynamic DSA intensity profiles. These indices can act as quantitative references to facilitate physicians' optical observation. (B) Individual flow indices correctly reflect a general trend to flow increase post treatment. Unfortunately, several local pixels for patient-3 and patient-4 show the complete opposite trend (flow decrease) after intervention. When assessing interventional outcomes based on simple flow indices caution is indicated, because inconsistencies cannot be avoided due to limitations in the data acquisition in conventional DSA.

ISSN 2473-0947 Open Journal http://dx.doi.org/10.17140/ROJ-1-104

patients, the intensity based maps properly indicate successful intervention. Overall, the RCABi map of patient-3 shows improved blood flow even though the RCABi values for several individual pixels contradict the trend. The two-dimensional RCABi and TTPi map appear to be more robust than single pixel indices, because the spatial normalization eliminates individual outliers leading to more robust "integral" snapshot of the blood flow pattern compared the "local" RCABi and TTPi.

Thus, intensity-based maps are better suited for the assessment of interventional outcomes. Yet, even the maps cannot render absolute blood flow rates in individual vessels.

Flow Inversion from Reconstructed DSA

We also estimated blood flow rates in patient-2 and patient-4 using a novel inversion technique for DSA images. Measured contrast concentration profiles were compared to the simulated trajectories to obtain blood pressure and volumetric flow rates. During an iterative procedure, the inversion model chooses suitable inlet pressures, which in turn affects the flow rates, as well as the dynamically simulated contrast agent intensity profiles throughout the network. The boundary pressures and indirectly the flow rates that lead to the best alignment between the simulated contrast agent concentration profiles with the measured intensity profiles from DSA are deemed the optimal solution. The optimal solution minimizes the objective function in (1) which is the difference between measured and simulated contrast agent profiles. We assumed a linear relationship between intensity and contrast agent concentrations. The side conditions include the continuity in (2), pressure drop according to Hagen Poiseuille law in (3) and the dynamics of contrast agent distribution by blood advection in (4). The information flow of the inversion model is shown in Figure 4. The problem of minimizing (1) subject to (2-4) is a non-linear mathematical program (NLP) with partial differential constraints. We solved the NLP after time discretization with a one-step implicit Euler method with step size t=100 ms with genetic algorithm (GA) optimizer in MATLAB, details on GA optimizer can be found elsewhere.[35] Optimization parameters were set to population size=1000, number of iterations=500. Typical computation time for the inversion model did not exceed 20 CPU seconds on an Intel Core2Duo E8400. The intensities for the optimization were taken from the arterial phase only, background noise was filtered by subtracting the intensity of a contra-lateral hemisphere, and the area under the curve of the intensity was normalized to a unity. The final solution with the best match between the concentration profiles yields the desired volumetric flow rates. The pressure drops and the simulated concentrations profiles are simultaneous outcomes of the inversion procedure.

Optimal Flow From Inversion Of The Intensity Profiles

For the inversion of the contrast agent profiles, the inlet contrast concentration was set equal to the actual contrast infusion profile acquired at the first segment of the ICA. The optimal solution of flow rates from inversion are shown in Figure 5C, 5D and compared well with the QMRA measurements. The optimal flow rates were independent of the initial guesses for the unknown pressures and flows during the inversion. Figure 5B also shows

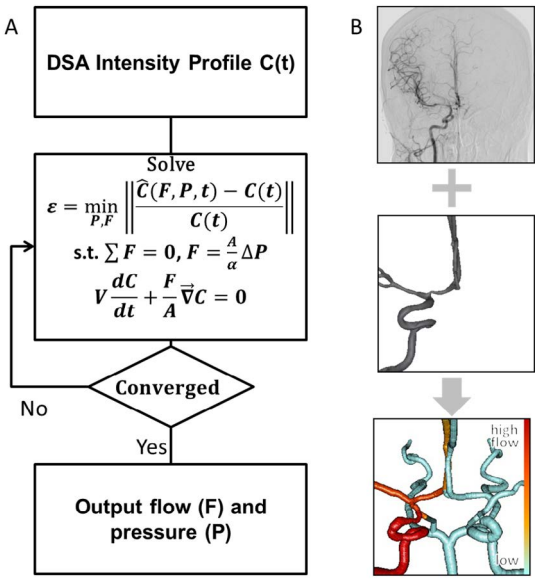

Figure 4. Information flow for novel inversion technique for estimating cerebral blood flow in large arteries with fractional DSA. The inversion consists in solving a non-linear optimization problem which minimizes the difference between measured and simulated intensity profiles. The optimal solution determines the flow rates and pressures that give the best alignment between measurements and model B. Intensity profiles are extracted from DSA images (top). Anatomical information about the patient-specific network of main cerebral arteries is derived from medical images (middle). Flow results from inversion of the DSA images. The red gradient color bar indicates the volumetric flow rates; vessels in white are unavailable from DSA reconstruction (bottom).

ISSN 2473-0947 Open Journal http://dx.doi.org/10.17140/ROJ-1-104

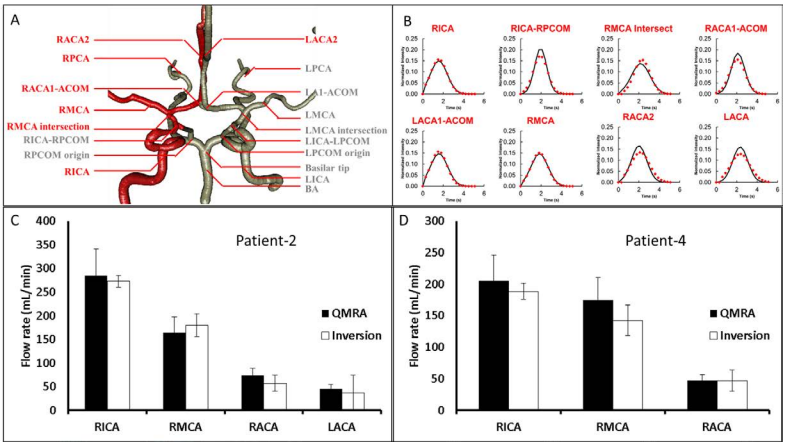

Figure 5. Flow estimation from inversion-based model. A. An anatomical network model of the main blood arteries in the right hemisphere was reconstructed from constant infusion DSA and used for the hemodynamic computations into contrast advection during the inversion procedure. Red labels and vessels indicate positions examined in patient-4, grey labels and vessels mark other anatomical areas. B. Intensity profiles extracted from DSA at the RICA, RMCA, RACA, and LACA (dots) used in the inversion-base flow rate assessment. Crude intensity data were considered during the arterial phase, background was subtracted and the area under the curve for each intensity plot was normalized to unity. Solid lines show the simulated intensity profiles of the optimal solution. The good alignment between the two curves supports the validity of the flow estimation. C. The flow estimation with the novel inversion technique compared to the golden standard of QMRA for patient-2. Flow estimation from inversion-based model in vessels of interest is within 25% difference of QMRA. D. The flow estimation with the novel inversion technique compared to the golden standard of QMRA for patient-4. Flow estimation from inversion-based model in vessels of interest lies within 25% of the QMRA value.

the intensity profiles in simulation and actual DSA data sets in good qualitative and quantitative agreement. The absolute volumetric flow rates were computed by inversion as 263.6 mL/min in the RICA, 168.5 in the RMCA, 56.5 in the RACA, and 38.5 in the LACA. Compared to NOVA, there are only small differences: 2.7% in the RICA, 8.9% in the RMCA, 23.2% in the RACA, and 9.5% in the LACA. The inversion model renders the desired flow rate estimates. It implicitly performs smoothing of the noisy contrast agent intensity data based on fluid dynamic principles. Incorporation of flow physical principles into the noise reduction seems advantageous when compared to *uninformed* data fitting used in conventional deconvolution.

Confidence Regions of Flow Estimation

We also computed the individual confidence intervals to assess the reliability of the flow estimation. Independent confidence intervals for confidence level of 99% were calculated based on the covariance method described in.[36] The covariance method requires the

sensitivity information; the elements of the Jacobian matrix were computed numerically by repeated simulations with small changes to the flow rates in (5-7) with n is the number of observations, p is the number of parameters, V the covariance matrix, σ the individual variances, ε is the vector of concentration differences between the measurement and the model prediction with t as the student t-value. We computed for four different flow rates with eighty observations, and using 2.63 as t-value with 99% confidence. The final estimate for the blood flow in the RICA was 263.6±2.6 ml/min, 168.5±4.0 in the RMCA, 56.5±2.5 in the RACA, and 38.5±4.8 in the LACA, indicated as error bars in Figure 5C. We also reconstructed an anatomical network for the main arteries connected to the right hemisphere of the Circle of Willis for patient-4 and conducted flow measurements with the inversion technique described above. The flow estimation for patient-4 gave absolute volumetric flow rates of 182.9±6.1 mL/min in the RICA, 136.6±6.0 in the RMCA and 50.1±6.2 in the RACA as shown in Figure 5D. In comparison to the QMRA measurement were 205 mL/min, 175, and 49, respectively. The differences between flow rates acquired with inversion of traditional DSA and QMRA were smaller than 25%.

$$J = \begin{bmatrix} \frac{\partial C_1}{\partial F_1} & \cdots & \frac{\partial C_1}{\partial F_4} \\ \vdots & \ddots & \vdots \\ \frac{\partial C_{80}}{\partial F_1} & \cdots & \frac{\partial C_{80}}{\partial F_4} \end{bmatrix} \quad (5)$$

$$V_F = s^2 \left[J\left(\hat{F}\right)^T J\left(\hat{F}\right) \right]^{-1} = \frac{\varepsilon^T \varepsilon}{n-p} \left[J\left(\hat{F}\right)^T J\left(\hat{F}\right) \right]^{-1} \quad (6)$$

$$\left| F_i - \hat{F}_i \right| \leq \sqrt{\sigma_{ii,\hat{F}}} \cdot t_{n-p,1-\frac{\gamma}{2}} \quad (7)$$

DISCUSSION

Intensity-based indices are appealing for the clinical practice especially during the interventional setting due to their ease of use. In this paper, two intensity-based angiographic indices, time-to-peak (TTPi) and relative cerebral angiographic blood flow index (RCABi) were investigated in four patients requiring neurovascular interventions. In all cases, improvements after neurovascular intervention were correctly detected by the TTPi. The RCABi analysis of two patients failed to reflect the correct trend. Such mismatches would not be acceptable for clinical outcome evaluations. We conclude that caution must be exercised when using angiographic intensity-based indices even for qualitative outcome assessment of neurosurgical

interventions.

In addition, the quantitative correlation between intensity-based indices and absolute blood through individual arteries was found to be weak (R^2<0.7). The imprecision is due to the low acquisition rate of DSA, the overlap of intensity in the angiographic projection planes, secondary injection of contrast agent, and attenuation of intensity through bony structures. The degree of variability and uncertainty is also a function of the patient-specific flow patterns. The use of these indices is reasonable as indirect assessment of relative change in blood flow post intervention (angioplasty, stenting, infusion of vasodilators, dural fistula or arteriovenous embolization), while the patient is still in the angiography suite. Especially the blood flow assessment for patients with flow reversal may be susceptible to incorrect trends as was the case in patient-3.

Two-dimensional TTPi and RCABi maps were found to be more robust than point measurements. The comparison of maps pre- and post- intervention reflected correctly the qualitative improvement in all four cases. The apparent improved reliability of two-dimensional index maps over the local indices can be attributed to the spatially integral character of the map. The spatially distributed RCABi or TTPi fields better reflects the global flow pattern, and appears less sensitive to errors than local indices evaluated for individual pixels. However, even flow index maps also do not render absolute volumetric flow rates.

To overcome the limitation of quantifying blood flow in conventional DSA, we presented a novel inversion technique that incorporates patient-specific anatomy in the image analysis. In two patients, DSA based blood flow measurement were demonstrated using an anatomically consistent hemodynamic model around the main arteries in the injected hemisphere. Using this patient-specific blood flow network and measured intensity plots from DSA as input, the inversion technique yielded absolute blood flow estimates within 25% of the QMRA NOVA measurements. Computation time needed for inverting the concentration profile were less than 20 seconds which shows that the inversion-based absolute flow estimation can be solved in real-time.

Unavoidable measurement error is attributable to the intensity overlap in the DSA projections, and noise during image acquisition. There is also mismatch between actual injection dynamics causing complex mixing patterns and the simplified flow assumptions used for the inversion. Fast contrast infusion creates a jet which carries the contrast agent initially much faster than shortly afterwards when the blood flow returns to normal. In DSA with limited frame acquisition rate, the rapid initial contrast agent ejection is an unavoidable source of error especially close to the injection site.

For building the hemodynamic model, patient-specific DSA images after constant infusion into one hemisphere were available in this study. The lack of observations for the contra-lateral side is expected to affect the estimation error. To quantify the effect of this error, we also built a complete intracranial vasculature model from patient-specific MRA images to perform the same flow estimation by inversion of a complete Circle of Willis and bilateral main cerebral arteries. The inversion result was within 20% of the QMRA results. The results from complete network inversion differed by only 5% from the hemispherical predictions. This preliminary study demonstrates the feasibility of acquiring absolute blood flow rates in large arteries with conventional DSA with an inversion technique that incorporates anatomical details in the image analysis of dynamic contrast profiles.

CONCLUSIONS

DSA is an established technique for hemodynamic assessment in an emergency clinical setting, which currently lacks volumetric blood flow rate estimation to ascertain the effectiveness of the neurovascular intervention. The limitations of two intensity-based flow indices for neurovascular intervention assessment were highlighted. Two-dimensional maps based on intensity-based indices were found more robust against misinterpretation.

A novel inversion technique to measure absolute flow in major arteries accounting for patient-specific anatomy in addition to DSA contrast agent profiles was introduced. The novel methods incorporated fluid mechanical and transport physics into the medical image analysis of DSA dynamic contrast data. The proposed inversion technique seems to give good flow estimates by smoothing the noisy image data according to hemodynamic principles. The combination of intensity profiles and patient-specific flow network is a promising approach to render absolute blood flow measurements with traditional DSA.

ACKNOWLEDGMENTS

The authors would like to gratefully acknowledge NIH for their financial support of this project, NIH-5R21EB004956. No conflicts of interest were posed in the conduct of this research.

CONFLICT OF INTEREST: None.

REFERENCES

1. Go AS, Mozaffarian D, Roger VL, et al. Executive summary: heart disease and stroke statistics--2013 update: a report from the American Heart Association. *Circulation.* 2013; 127(1):143-152. doi: 10.1161/CIR.0b013e318282ab8f

2. van Rooij WJ, Sluzewski M, Slob MJ, Rinkel GJ. Predictive value of angiographic testing for tolerance to therapeutic occlusion of the carotid artery. *AJNR Am J Neuroradiol*. 2005; 26(1): 175-178. Web site. http://www.ajnr.org/content/26/1/175.long. Accessed April 14, 2016

3. Macdonald RL, Wallace MC, Kestle JR. Role of angiography following aneurysm surgery. *J neurosurg*. 1993; 79(6): 826-832. Web site. http://thejns.org/doi/abs/10.3171/jns.1993.79.6.0826. Accessed April 14, 2016

4. Chiang VL, Gailloud P, Murphy KJ, Rigamonti D, Tamargo RJ. Routine intraoperative angiography during aneurysm surgery. *J neurosurg*. 2002; 96(6): 988-992. Web site. http://thejns.org/doi/abs/10.3171/jns.2002.96.6.0988. Accessed April 14, 2016

5. Tang G, Cawley CM, Dion JE, Barrow DL. Intraoperative angiography during aneurysm surgery: a prospective evaluation of efficacy. *J neurosurg*. 2002; 96(6): 993-999. Web site. http://thejns.org/doi/abs/10.3171/jns.2002.96.6.0993?url_ver=Z39.88-2003&rfr_id=ori:rid:crossref.org&rfr_dat=cr_pub%3dpubmed. Accessed April 14, 2016

6. Zhao M, Amin-Hanjani S, Ruland S, Curcio AP, Ostergren L, Charbel FT. Regional cerebral blood flow using quantitative MR angiography. *AJNR Am J Neuroradiol*. 2007; 28(8): 1470-1473. doi: 10.3174/ajnr.A0582

7. Bauer AM, Amin-Hanjani S, Alaraj A, Charbel FT. Quantitative magnetic resonance angiography in the evaluation of the subclavian steal syndrome: report of 5 patients. *J Neuroimaging*. 2009; 19(3): 250-252. doi: 10.1111/j.1552-6569.2008.00297.x

8. Mallett BL, Veall N. Investigation of cerebral blood-flow in hypertension, using radioactive-xenon inhalation and extracranial recording. *Lancet*. 1963; 281(7290): 1081-1082. doi: 10.1016/S0140-6736(63)92116-0

9. Chiron C, Raynaud C, Tzourio N, et al. Regional cerebral blood flow by SPECT imaging in Sturge-Weber disease: an aid for diagnosis. *J Neurol Neurosurg Psychiatry*. 1989; 52(12): 1402-1409. Web site. http://jnnp.bmj.com/content/52/12/1402.long. Accessed April 14, 2016

10. Iida H, Itoh H, Nakazawa M, et al. Quantitative mapping of regional cerebral blood flow using iodine-123-IMP and SPECT. *J Nucl Med*. 1994; 35(12): 2019-2030. Web site. http://jnm.snmjournals.org/content/35/12/2019.long. Accessed April 14, 2016

11. Demirkaya S, Uluc K, Bek S, Vural O. Normal blood flow velocities of basal cerebral arteries decrease with advancing age: a transcranial Doppler sonography study. *Tohoku J Exp Med*. 2008; 214(2): 145-149. doi: 10.1620/tjem.214.145

12. Ibaraki M, Ito H, Shimosegawa E, et al. Cerebral vascular mean transit time in healthy humans: a comparative study with PET and dynamic susceptibility contrast-enhanced MRI. *J Cereb Blood Flow Metab*. 2007; 27(2): 404-413. doi: 10.1038/sj.jcbfm.9600337

13. Parsons MW. Perfusion CT: is it clinically useful? International journal of stroke : official journal of the International Stroke Society. 2008; 3(1): 41-50.

14. Allmendinger AM, Tang ER, Lui YW, Spektor V. Imaging of stroke: Part 1, Perfusion CT--overview of imaging technique, interpretation pearls, and common pitfalls. *AJR Am J Roentgenol*. 2012; 198(1): 52-62. doi: 10.2214/AJR.10.7255

15. Kamalian S, Kamalian S, Konstas AA, et al. CT perfusion mean transit time maps optimally distinguish benign oligemia from true "at-risk" ischemic penumbra, but thresholds vary by postprocessing technique. *AJNR Am J Neuroradiol*. 2012; 33(3): 545-549. doi: 10.3174/ajnr.A2809

16. Fieselmann A, Ganguly A, Deuerling-Zheng Y, Zellerhoff M, Rohkohl C, Boese J, et al. Interventional 4-D C-arm CT perfusion imaging using interleaved scanning and partial reconstruction interpolation. *IEEE Trans Med Imaging*. 2012; 31(4): 892-906. doi: 10.1109/TMI.2011.2181531

17. Fieselmann A, Kowarschik M, Ganguly A, Hornegger J, Fahrig R. Deconvolution-Based CT and MR Brain Perfusion Measurement: Theoretical Model Revisited and Practical Implementation Details. *Int biome imaging*. 2011; 2011: 467563. doi: 10.1155/2011/467563

18. Zhang C, Villa-Uriol MC, De Craene M, Pozo JM, Macho JM, Frangi AF. Dynamic estimation of three-dimensional cerebrovascular deformation from rotational angiography. *Med phys*. 2011; 38(3) :1294-1306. doi: 10.1118/1.3549761

19. Waechter I, Bredno J, Barratt DC, Weese J, Hawkes DJ. Quantification of blood flow from rotational angiography. *Med Image Comput Comput Assist Interv*. 2007; 10(Pt 1): 634-641. doi: 10.1007/978-3-540-75757-3_77

20. Waechter I, Bredno J, Hermans R, Weese J, Barratt DC, Hawkes DJ. Model-based blood flow quantification from rotational angiography. *Med image anal*. 2008; 12(5): 586-602. doi: 10.1016/j.media.2008.06.003

21. Tenjin H, Asakura F, Nakahara Y, et al. Evaluation of intraaneurysmal blood velocity by time-density curve analysis and digital subtraction angiography. *AJNR Am j neuroradiol*. 1998; 19(7): 1303-1307. Web site. http://www.ajnr.org/content/19/7/1303.long. Accessed April 14, 2016

22. Kamp MA, Slotty P, Turowski B, et al. Microscope-integrated quantitative analysis of intraoperative indocyanine green fluorescence angiography for blood flow assessment: first experience in 30 patients. Neurosurgery. 2012; 70(1 Suppl Operative): 65-73. doi: 10.1227/NEU.0b013e31822f7d7c

23. Divani AA, Lieber BB, Wakhloo AK, Gounis MJ, Hopkins LN. Determination of blood flow velocity and transit time in cerebral arteriovenous malformation using microdroplet angiography. *Ann Biomed Eng*. 2001; 29(2): 135-144. doi: 10.1114/1.1349696

ISSN 2473-0947 Open Journal http://dx.doi.org/10.17140/ROJ-1-104

24. Bursch JH, Hahne HJ, Brennecke R, Gronemeier D, Heintzen PH. Assessment of arterial blood flow measurements by digital angiography. *Radiol*. 1981; 141(1): 39-47. doi: 10.1148/radiology.141.1.7291540

25. Molloi S, Zhou Y, Kassab GS. Regional volumetric coronary blood flow measurement by digital angiography: in vivo validation. *Acad radiol*. 2004; 11(7): 757-766. doi: 10.1016/j.acra.2004.04.002

26. Hangiandreou NJ, Folts JD, Peppler WW, Mistretta CA. Coronary blood flow measurement using an angiographic first pass distribution technique: a feasibility study. *Med phys*. 1991; 18(5): 947-954. doi: 10.1118/1.596716

27. Huang SP, Decker RJ, Goodrich KC, Parker DJ, Muhlestein JB, Blatter DD, et al. Velocity measurement based on bolus tracking with the aid of three-dimensional reconstruction from digital subtraction angiography. *Med phys*. 1997; 24(5): 677-686. doi: 10.1118/1.597990

28. Efron U, Price RR, Smith CW, Brill AB. A method to determine the instantaneous blood-flow using cine- or video-densitometric data. *Proc. SPIE 0143, Applications of Electronic Imaging Systems*. 1978: 154-161. doi: 10.1117/12.956561

29. Sarry L, Boire JY, Zanca M, Lusson JR, Cassagnes J. Assessment of stenosis severity using a novel method to estimate spatial and temporal variations of blood flow velocity in biplane coronarography. *Phys med biol*. 1997; 42(8): 1549-1564. Web site. http://iopscience.iop.org/article/10.1088/0031-9155/42/8/006/pdf. Accessed April 14, 2016

30. Shpilfoygel SD, Close RA, Valentino DJ, Duckwiler GR. X-ray videodensitometric methods for blood flow and velocity measurement: a critical review of literature. *Med phy*. 2000; 27(9): 2008-2023. doi: 10.1118/1.1288669

31. Lorensen WE, Cline HE. Marching cubes: A high resolution 3D surface construction algorithm. *SIGGRAPH Comput Graph*. 1987; 21(4): 163-169. doi: 10.1145/37401.37422

32. Piccinelli M, Veneziani A, Steinman DA, Remuzzi A, Antiga L. A framework for geometric analysis of vascular structures: application to cerebral aneurysms. *IEEE Trans Med Imaging*. 2009; 28(8): 1141-1155. doi: 10.1109/TMI.2009.2021652

33. Westerhof N, Stergiopulos N, Noble M. Snapshots of Hemodynamics: An aid for clinical research and graduate education; 2005.

34. Bui A, Sutalo ID, Manasseh R, Liffman K. Dynamics of pulsatile flow in fractal models of vascular branching networks. *Med Biol Eng Comput*. 2009; 47(7): 763-772. doi: 10.1007/s11517-009-0492-6

35. Moon J, Linninger AA. A hybrid sequential niche algorithm for optimal engineering design with solution multiplicity. *Comput Chem Eng*. 2009; 33(7): 1261-1271. doi: 10.1016/j.compchemeng.2009.02.006

36. Kulkarni K, Zhang LB, Linninger AA. Model and parameter uncertainty in distributed systems. *Ind Eng Chem Res*. 2006; 45(23): 7832-7840. doi: 10.1021/ie0604876

RADIOLOGY

Openventio PUBLISHERS

ISSN 2473-0947 Open Journal http://dx.doi.org/10.17140/ROJ-1-105

Research

*Corresponding author
Mario Sansone, PhD
Assistant Professor
Department of Electrical Engineering and Telecommunications
University of Naples "Federico II"
via Claudio 21
80131-Naples, Italy
Tel. +39 081 768 3807
E-mail: msansone@unina.it

Volume 1 : Issue 1
Article Ref. #: 1000ROJ1105

Article History
Received: May 16th, 2016
Accepted: May 24th, 2016
Published: May 24th, 2016

Citation
Sansone M, Fusco R, Petrillo A. An attempt to integrate diffusion weighted and dynamic contrast enhanced MRI. *Radiol Open J*. 2016; 1(1): 31-34. doi: 10.17140/ROJ-1-105

An Attempt to Integrate Diffusion Weighted and Dynamic Contrast Enhanced MRI

Mario Sansone, PhD[1*]; Roberta Fusco, PhD[2]; Antonella Petrillo, MD, PhD[2]

[1]Department of Electrical Engineering and Information Technologies, University of Naples "Federico II" via Claudio, 2180131 Naples, Italy
[2]Department of Diagnostic Imaging, National Cancer Institute, "G. Pascale" Foundation, Naples, Italy

ABSTRACT

Diffusion Weighted MRI (DWI) and Dynamic Contrast Enhanced MRI (DCE-MRI) are increasingly used for cancer assessment. Both modalities require adequate post-processing to extract useful information. DWI can be analyzed using the Intra-Voxel Incoherent Motion (IVIM) model while DCE-MRI can be analyzed using the Extended Tofts and Kermode (ETK) model. Both models have some parameters that can be estimated *via* numerical data-fitting procedures. The two mentioned models are typically fitted independently from each other. However, noise superimposed on images can affect the reliability of estimated parameters. In this feasibility study, we propose to exploit the link between the two models in order to possibly improve the quality of fitting. Preliminary results suggest that IVIM fitting can be improved when both ETK and IVIM are performed.

KEYWORDS: Diffusion weighted MRI; Dynamic contrast enhanced MRI; Intra-Voxel Incoherent Motion model; Extended Tofts-Kermode model; Simultaneous fitting.

INTRODUCTION

In cancer studies of several organs (e.g. breast, prostate, liver, etc…) functional imaging can give useful information for better quantify the staging. In particular, Diffusion Weighted Imaging (DWI) and Dynamic Contrast Enhanced (DCE) MRI are becoming increasingly adopted in clinical practice.

DWI can give information about the microstructure organisation of the tissue. In fact, tumors have an increased cellularity leading to reduced water diffusion.[1] Isotropic diffusion can be modeled using Intra-Voxel Incoherent Motion (IVIM)[2] which depends on a few parameters: perfusion fraction f (fraction of plasma vessels), 'slow' diffusion D_s (conventional diffusion), 'fast' diffusion D_f (diffusion in randomly oriented vessel). Diffusion constants are measured in mm^2/s.

DCE provides information on the capillary wall permeability. This latter increases in cancer because of leaky vessels associated to the fast grow induced by VEGF (vascular endothelial growing factor).[3] One of the most commonly employed models is the Extended Tofts-Kety (ETK) model[4] includes the following parameters: vascular plasma fraction (v_p), transfer constant from plasma to extra-vascular-extra-cellular space (EES) K^{trans}, transfer constant from EES to plasma k_{ep}. Transfer constant are mesured in min^{-1}.

Both models parameters are typically estimated from measured DCE and DWI data. Due to noise the estimated parameters can inaccurate and imprecise.

Following the suggestion by LeBihan et al.[5] in this study we hypothesized that perfusion fraction (f) in IVIM and plasma volume fraction (v_p) should be equal and might be

ISSN 2473-0947 Open Journal http://dx.doi.org/10.17140/ROJ-1-105

used for improving the estimation of parameters attainable with DWI and DCE.

In particular, we performed a Monte Carlo simulation in order to evaluate how the IVIM and ETK fitting can be performed simultaneously and if the simultaneous fitting can produce better performance than separate fitting.

METHODS

Intra-Voxel Incoherent Motion (IVIM) Modeling

The IVIM model has been proposed by Le Bihan et al[2] according to this model the signal intensity of the diffusion weighted images is given by: $S_{IVIM}(b) = S_0 \cdot [(1-f) \cdot \exp(-b \cdot D_s) + f \cdot \exp(-b \cdot D_f)]$. where S0 is the signal intensity with no diffusion gradient, f is the perfusion fraction, D_s is the slow diffusion coefficient of water and D_f is the 'fast' diffusion coefficient, b is the b-value that is related to the pulse magnetic gradient intensity and duration.

Extended Tofts And Kermode (ETK) Modeling

Tofts and Kermode proposed a model for the capillary flow.[4] According to this model the concentration of contrast agent within a voxel is given by: $S_{ETK}(t) = v_p \cdot C_p(t) + C_p(t) \star K^{trans} \cdot e^{-k_{ep}t}$ where t is time, K^{trans} min^{-1}. is the transfer constant across the capillary wall from the plasma to the Ees, k_{ep} is the reverse constant from EES to plasma, v_p is the plasma volume fraction.

Simultaneous Fitting Of IVIM And ETK

Le Bihan et al[5] suggested that the perfusion fraction within the IVIM model should be interpreted as the vessel fraction within a voxel. This hypothesis, might be used to improve the numerical estimation of model parameters (DWI and DCE) performing simultaneous fitting of both data.

In order to take advantage of the link between IVIM and ETK models we need to perform a simultaneous fit of the data. In this study we propose to perform minimization of an appropriate cost function. Under the hypothesis that $f=v_p$ the cost function can be written:

$$C(f, D_s, D_f, K^{trans}, k_{ep}) = \sum_b (S_{IVIM}(b, f, D_s, D_f) - S_{DWI}(b))^2 + \sum_t (S_{ETK}(t, f, K^{trans}, k_{ep}) - S_{DCE}(t))^2$$

where $S_{DWI}(b)$ is the signal acquired during DWI and $S_{DCE}(t)$ is the signal acquired during DCE-MRI.

SIMULATIONS

We simulated one ETK curve with K^{trans}=0.046 min^{-1}. and k_{ep}=0.148 min^{-1}. and v_p=0.0074. The parker model for the arterial input function has been used.[6] Time sampling was simulated as in fast TWIST (Time-resolved angiography With Interleaved Stochastic Trajectories) pulse sequences with an image every 3 sec. Noise was superimposed having a standard deviation of 0.1 mMol.

Further we simulated a IVIM curve using $f=v_p$=0.0074, D_s=0.001 mm^2/s, D_f=0.01 mm^2/s and b-values (0, 50, 100, 150, 200, 500, 600, 700, 800, 900, 1000, s/mm^2). Noise was simulated having standard deviation 0.05 normalised units.

Simultaneous fitting using the cost function proposed in the previous section has been performed. Starting values were: K^{trans}=1, k_{ep}=0.5, v_p=f=0.5, D_s=1e-3, D_f=10e-3. The Levenberg-Marquardt algorithm in Matlab has been used.

Monte Carlo simulation on 10 repetitions has been performed on the same noisy data but with different starting points chosen randomly within 10% of the starting values reported in the previous paragraph.

RESULTS

Figures 1 and 2 report the simulated curves with superimposed

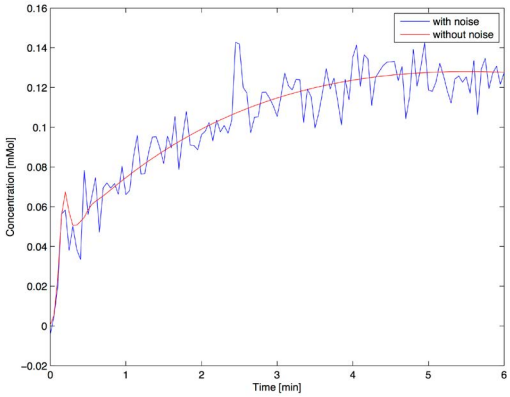

Figure 1: DCE simulated data without and with noise superimposed. It is assumed that a fast pulse sequence is used (e.g. such as TWIST[7]) capable to acquire an image every 3 seconds. The noise level (std) has been fixed to 0.01 mMol. Noise distribution was assumed zero-mean Gaussian.

ISSN 2473-0947 Open Journal http://dx.doi.org/10.17140/ROJ-1-105

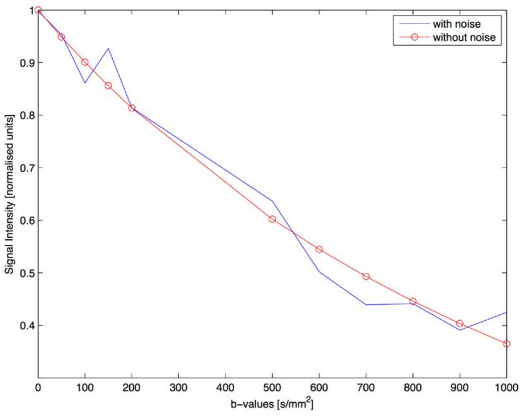

Figure 2: DWI simulated data without and with noise superimposed. It is assumed that a typical range of b-values has been used (0, 50, 100, 150, 200, 500, 600, 700, 800, 900, 1000, s/mm²). The noise level (std) has been assumed 0.05 normalized units. Noise distribution has been assumed zero-mean Gaussian.

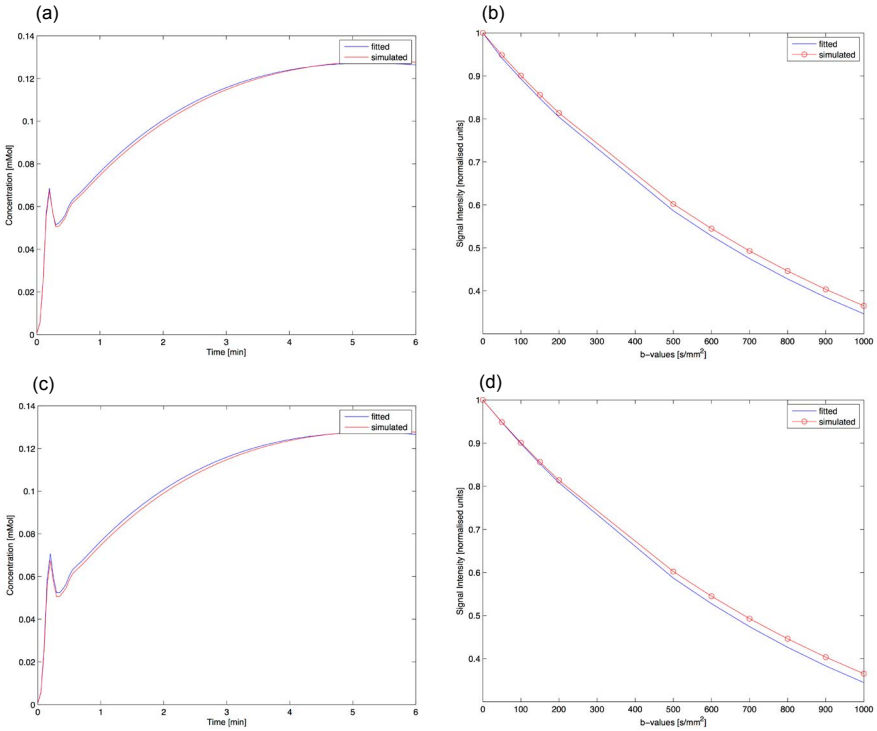

Figure 3: (a) and (b) fitting using the cost function proposed combining DCE and DWI. (c) and (d) fitting separately DCE and DWI.

noise. Figure 3 report the result of fitting using the proposed cost-function (Figures a and b) , and separately fitting the data (Figures c and d).

When using simultaneous cost-function, mean relative error (expressed in percentage %) on parameters were: K^{trans}=-7.20%, k_{ep}=11.54 %, v_p=f=21.01%, D_s=-5.1132%, D_f= -99.9850%. When the fitting were performed separately mean percentage errors were: K^{trans} = -3.75 %, k_{ep}=6.37% v_p=4.25% for the ETK model and f=6*10⁶%, D_s=6.13%, D_f= 347%.

DISCUSSION

In this study we explored the possibility to perform simultaneous fitting of DCE and DWI data under the hypothesis that plasma fraction and perfusion fraction are the same as suggested by Le Bihan et al.[5] We performed Monte Carlo simulations with noisy DCE and DWI data. Simulated data were fitted separately and in combination.

Results suggest that DCE fitting can lead to better

ISSN 2473-0947 Open Journal http://dx.doi.org/10.17140/ROJ-1-105

results when performed alone. However, DWI data fitting can lead to huge errors in parameter estimates that might be attenuated when fitted simultaneously with DCE data.

Although results seems promising, we must underline the limits of this study. In our study we did not evaluate the impact of different curve fitting algorithms, the influence of the noise level, the influence of the number of b-values used.

It seems reasonable that a larger number of b-values might improve DWI fitting alone and consequently also the combined fitting.

CONFLICTS OF INTEREST: None.

REFERENCES

1. Koh D-M, Collins DJ. Diffusion-weighted MRI in the body: applications and challenges in oncology. *Am J Roentgenol*. 2007; 188(6): 1622-1635. doi: 10.2214/AJR.06.1403

2. Le Bihan D, Breton E, Lallemand D, Grenier P, Cabanis E, Laval-Jeantet M. MR imaging of intravoxel incoherent motions: application to diffusion and perfusion in neurologic disorders. *Radiology*. 1986; 161(2): 401-407. doi: 10.1148/radiology.161.2.3763909

3. Sourbron SP, Buckley DL. On the scope and interpretation of the Tofts models for DCE-MRI. *Magn Reson Med*. 2011; 66(3): 735-745. doi: 10.1002/mrm.22861

4. Tofts PS, Kermode AG. Measurement of the blood-brain barrier permeability and leakage space using dynamic MR imaging. 1. Fundamental concepts. *Magn Reson Med*. 1991; 17(2): 357-367.doi: 10.1002/mrm.1910170208

5. Le Bihan D, Turner R. The capillary network: a link between IVIM and classical perfusion. *Magn Reson Med.* 1992; 27(1): 171-178. Web site: http://meteoreservice.com/PDFs/LeBihan92.pdf. Accessed April 14, 2016

6. Parker GJ, Roberts C, Macdonald A, et al. Experimentally-derived functional form for a population-averaged high-temporal-resolution arterial input function for dynamic contrast-enhanced MRI. *Magn Reson Med*. 2006; 56(5): 993-1000. doi: 10.1002/mrm.21066

7. Sansone M, Fusco R, Petrillo A. Accuracy of contrast agent quantification in MRI: a comparison between two k-space sampling schemes applied magnetic resonance. *Applied Magnetic Resonance*. 2015; 46(11): 1283-1292. doi: 10.1007/s00723-015-0718-8